

REVIEW ARTICLE

Open Access



Advances of LINAC-based boron neutron capture therapy in Korea

Young-soon Bae^{1,2*}, Dong-Su Kim^{1,2}, Hyo Jung Seo², Je-Un Han^{1,2}, Hyung Jin Yoon^{1,2}, Jung Jin Hwang^{1,2}, Ju Jin Kim^{1,2}, Byung Hyo Woo¹, Hyo Jin Kim^{1,2}, Yoo Soon Jang¹, Seok Chang Han², Woong Hee Kim^{1,2}, Do Goo Kang^{1,2}, Hyun Jin Seo¹, Soo Young Lee^{1,2}, Sang June Jeon², Jungyu Yi², Jeongwoo Lee², Il Hyeok Seo², Se Hyun Kim², Woo Hyoung Kim², Na Hyung Park¹, Myeng Hyun Lee¹, Sung June Bae¹, Seung Hoon Lee¹, Gyu Ho Cho¹, Seong Han Kim², Seong Hwan Moon¹, Min Kyu Lee², Jae Won Choi², Kyu Young Lee², Dong Seok Huh², Dong Woo Kim², Kyung June Min², Hyoung Min Yoon², Hyunhye Kyung², Jieun Yang², Dasom Na², Sangbong Lee², Jaehwan Han², Yongho Kwak², Sei-Young Lee², Joo Young Nam², Byung-Ho Choi¹, Young-Kwan Moon², Won Do², Mooyoung Yoo² and Sun-Sun Park^{1,2}

Abstract

Boron neutron capture therapy (BNCT) has been attracting interest as a new radiation modality for cancer therapy because it can selectively destroy cancer cells while maintaining the healthy state of surrounding normal cells. Many experimental trials have demonstrated significant BNCT treatment efficacy using neutron beams from research reactors. However, nuclear reactor technology cannot be scaled to sites in hospitals delivering patient treatment. Therefore, compact accelerator-based neutron sources that could be installed in many hospitals are under development or have even been commissioned at many facilities around the world. In Korea, a radio-frequency (RF) linac-based BNCT (A-BNCT) facility is under development by DawonMedax (DM). It provides the highly efficient production of an epithermal neutron beam with an optimized neutron energy spectrum range of 0.1~10 keV. With a 2-mA 10-MeV proton beam from the accelerator, the irradiation port epithermal neutron flux is higher than 1×10^9 n/cm²·s. Comprehensive verification and validation of the system have been conducted with the measurement of both proton and neutron beam characteristics. Significant therapeutic effects from BNCT have been confirmed by DM in both in vitro and in vivo non-clinical trials. Further, during exposure to epithermal neutrons, all other unintended radiation is controlled to levels meeting International Atomic Energy Agency (IAEA) recommendations. Recently, the Korean FDA has accepted an investigational new drug (IND) and the first-in-human clinical trial of BNCT is now being prepared. This paper introduces the principles of BNCT and accelerator-based neutron sources for BNCT and reports the recent advances of DM A-BNCT facility which is the main part of this paper.

1 Introduction

Boron neutron capture therapy (BNCT) has been attracting interest as a new modality for radiation cancer therapy. BNCT is unique in that it enables the biological targeting of cancer at a cellular level. That is, cancer

cells can be selectively destroyed without damaging surrounding normal cells. Therefore, BNCT is especially promising in the treatment of intractable cancer such as malignant brain tumors and recurrent cancers because of low collateral radiation damage [1].

BNCT uses a nuclear capture reaction between a thermal neutron beam and boron-10 (¹⁰B) in the cell. The reaction then emits a helium-4 nucleus (alpha particle) and a lithium-7 (⁷Li) nucleus into the cancer cell, with kinetic energies of 1.47 MeV and 0.84 MeV, respectively.

*Correspondence: ysbae@dawonsys.com

² DawonMedax, Seoul 06735, Korea

Full list of author information is available at the end of the article



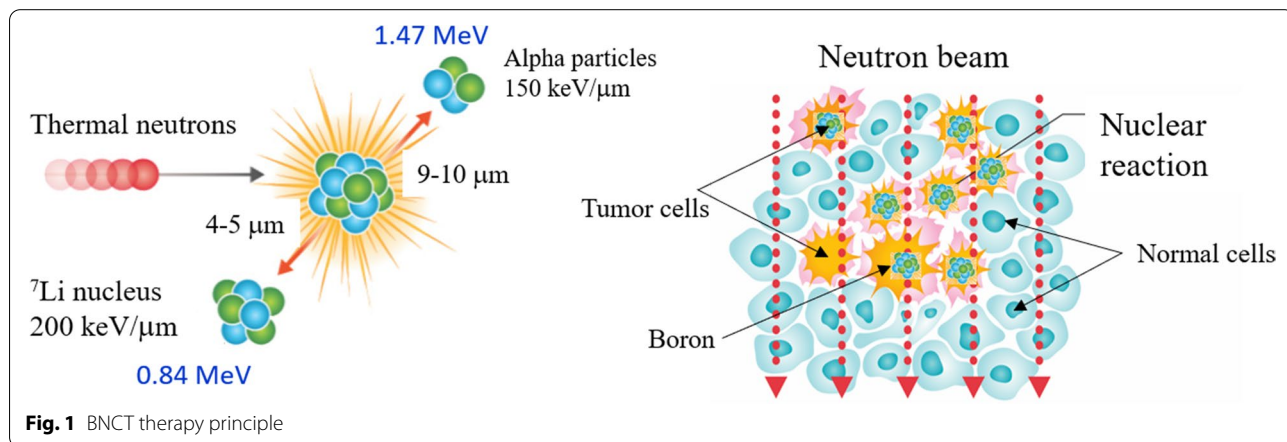
The two emitted nuclei feature a high “linear energy transfer (LET).” The high LET makes them densely ionizing particles which are more destructive to biological cells than low-LET radiation and particles. It is known that a LET of about 100 keV/μm is optimal for producing a high relative biological effectiveness (RBE), roughly a measure of the probability of causing DNA double-strand breaking (DSB) by the passage of a single charged particle [2]. More precisely, RBE is the relative biologic effect of the test radiation (*r*) as compared with X-rays and is defined by the ratio D_{250}/D_r , where D_{250} and D_r are, respectively, the doses of 250 keV X-rays and the test radiation required to produce an equal biologic effect [2]. The LET of the BNCT alpha particle is very close to this optimal value. Therefore, BNCT can be a solution to the problem of radiation-resistant cancers. In addition, owing to their high LET, the ranges of both particles in tissue are less than 10 μm, which is comparable to the size of a typical tumor cell. Therefore, using both particles from the BNCT-boron interaction, invasive tumor cells infiltrating healthy tissue can be selectively destroyed at the cellular level [3]. Figure 1 gives a pictorial summary of how BNCT works.

To obtain this nuclear reaction between thermal neutrons and ^{10}B , ^{10}B has to be first delivered to the cancer cells using a boron carrier compound, commonly called a boron agent. Therefore, the key components in BNCT are a supply of high-intensity neutrons and a boron drug delivery system with high uptake by cancer cells. The multiple desired requirements in boron delivery agents are a low normal tissue uptake but high tumor tissue uptake, the boron concentration in the tumor is recommended to be $\sim 20 \mu\text{g } ^{10}\text{B/g}$ tumor tissue, tumor-normal tissue (T/N) and tumor-blood (T/B) boron concentration ratios of not less than 3, rapid clearance from the blood and normal tissues, low systemic toxicity, and a constant concentration in the tumor during BNCT [4, 5].

Currently, the most widely used boron delivery agent for BNCT clinical trials is boronophenylalanine (BPA). BPA is a compound of amino acid phenylalanine bound to a single atom of boron. The boron content of BPA is about 5% by molecular weight.

Next, we consider the epithermal neutron source for BNCT. Originally, the only sources for neutron beams with sufficient intensity were research reactors. Clinical trials have been conducted around the world using research reactors for neutron sources since the 1960s: MITR at MIT, BMRR at BNL both in the USA; Petten HFR in the Netherlands; FiR1 at VTT in Finland; RA-6 at CNEA in Argentina; THOR at Tsinghua University in Taiwan; BCTC in Beijing, China; and JRR-4 at JAERI and KUR at Kyoto University both in Japan. Currently, only four facilities are operating, KUR in Japan [6], RA-6 in Argentina [7], THOR in Taiwan [8], and BCTC in China [9]. However, in recent decades, a practical alternate source has arrived with the development of high-current low-energy particle accelerators of various types. These particle accelerators can produce an epithermal neutron beam suitable for BNCT when fitted with a target that depends on the particle beam energy.

While worldwide various accelerator concepts are under consideration, in all cases for an accelerator-based neutron source, a proton beam is used for neutron production. The proton beam energy ranges from 2.0 to 30 MeV in the current available accelerator-based BNCT (A-BNCT). For low-energy protons nearer to 2 MeV, a lithium target is used, and for higher-energy protons ranging from 8 to 30 MeV, a beryllium target is used. There are multiple pros and cons between the choices for neutron sources and targets. This paper is organized by the following sections: accelerator-based neutron sources including neutron beam characteristics and neutron production by two typical targets are reviewed in section 2, A-BNCT facility in Korea led by DM and its advances moving toward clinical trials



are described in sections 3 to 5, and summary in the last section.

2 Accelerator-based neutron sources

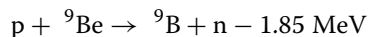
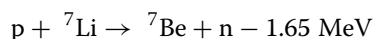
2.1 Neutron beam characteristic requirements for A-BNCT

Depending on the cancer types to be treated, different guidelines have been established setting the requirements for the neutron beam. For deep-seated cancers such as brain cancer, epithermal neutrons are suitable as the neutrons are moderated as they pass through the human body resulting in a high intensity of thermal neutrons arriving at the location of cancer. Even for superficial and shallow-seated cancers, such as melanoma and head and neck cancers, the use of an epithermal neutron beam can be acceptable if an additional moderator structure is provisioned at the irradiation beam port. The IAEA published a report with recommendations for BNCT neutron beam characteristics, TECDOC-1223 [10]. The guidelines found in TECDOC-1223 are mainly made based on BNCT treatment using a reactor neutron source. It is under revision to update to accelerator-based BNCT. The guideline focused on the treatment of deep-seated brain cancer and head and neck cancer. The neutron beam characteristics recommended in TECDOC-1223 are summarized in Table 1.

2.2 Neutron production

Proton accelerators have been used to generate neutron beams for accelerator-based BNCT. There are two targets, lithium and beryllium, depending on the proton beam energy which can generate a sufficient epithermal neutron flux.

For lithium, the reaction of ${}^7\text{Li}(p,n){}^7\text{Be}$ is used, while for beryllium, the reaction of ${}^9\text{Be}(p,n){}^9\text{B}$ is used. That is, the two typical nuclear reactions for neutron production for A-BNCT are as follows:



Both reactions are endothermic. The threshold energy of the proton-lithium (p-Li) reaction is 1.88 MeV and that of proton-beryllium (p-Be) is 2.06 MeV. The neutron yield from the nuclear reaction is defined as follows.

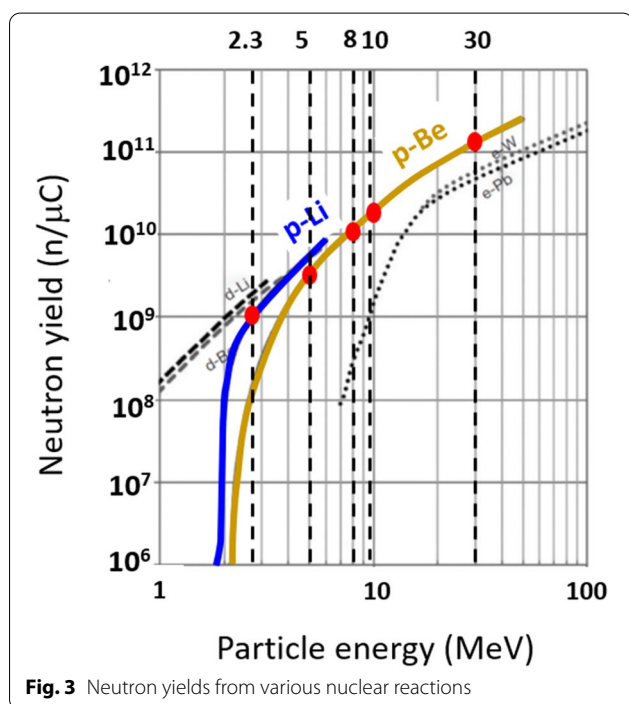
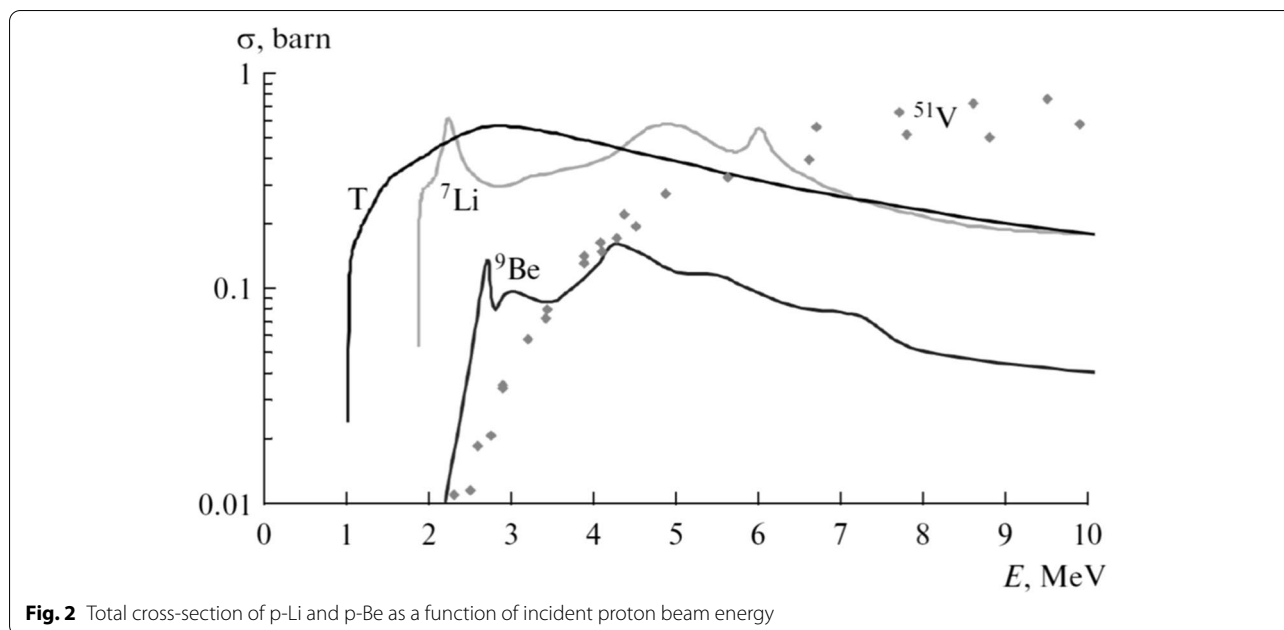
$$Y = \int_{E_i}^0 \int N_p(E) n_t \sigma(E) dV dE \tag{1}$$

where E_i is the initial kinetic energy of the bombarding particle, N_p is the number of incident particles, n_t is the density of the target material, and $\sigma(E)$ is the cross-section of the nuclear reaction as a function of bombarding particle energy. The neutron yield is a strongly nonlinear phenomenon that depends on the material properties. Figure 2 shows the total cross-section for nuclear reactions with p-Li and p-Be [11]. The total cross-section of the p-Li reaction is greatly elevated over the p-Be reaction. In the p-Li reaction, lower proton energy (2.1~2.5 MeV) is used instead of higher proton energy because there is a resonance peak in the cross-section around 2.3 MeV. Therefore, the resulting neutron energy is less than about 0.6 MeV. When the neutron energy exceeds 10 MeV, material activation is much higher with consequences to radiation safety, material handling, and decommissioning expenses. Thus, the lithium reaction has a great advantage in producing less radioactivity in the moderator system. Also, needing a lower-energy accelerator provides many benefits.

The total neutron yield of the p-Li reaction increases with the incident proton beam energy as seen in Fig. 3 [12]. In this figure, the target thickness is assumed to be sufficiently thick such that the incident proton beam is stopped completely inside the target. However, to maximize yield, the thickness of the lithium target should be increased up to the threshold limit of the p-Li reaction. But with a thick lithium target, it is not easy to provide enough cooling to keep the lower surface temperature below the melting point of 180 °C; this is because of lithium's very low thermal conductivity (about one fifth of that of copper). But, for example, at a lower proton energy of 2.3 MeV, the thickness where the threshold limit of p-Li reaction occurs is nearly 0.1 mm. Being so thin, cooling could be managed. However, a much higher proton current, up to 30 mA, would be needed to satisfy the required epithermal flux. Such a high thermal load would be difficult to manage even for a thin lithium target. How to keep the target below the melting point? Some ideas have been suggested to solve this difficulty, such as a rotating target [13], or increasing the beam energy up to 2.5 MeV while simultaneously decreasing the beam current. At the same time, the lithium target is chemically very active, and it changes into ${}^7\text{Be}$, which is a radioactive isotope emitting 478 keV γ -radiation with a

Table 1 Recommended neutron beam characteristics from IAEA TECDOC-1223

Beam characteristics	Recommended value
Neutron beam energy range (epithermal)	0.5 eV < E < 10 keV
Epithermal neutron flux, Φ_{epi}	$\geq 1 \times 10^9 \text{ n/cm}^2 \cdot \text{s}$
Fast neutron contamination (fast neutron dose/ Φ_{epi})	$\leq 2 \times 10^{-13} \text{ Gy} \cdot \text{cm}^2$
γ -ray contamination (γ -ray dose/ Φ_{epi})	$\leq 2 \times 10^{-13} \text{ Gy} \cdot \text{cm}^2$
Thermal neutron ratio	≤ 0.05
Current to flux ratio	≥ 0.7



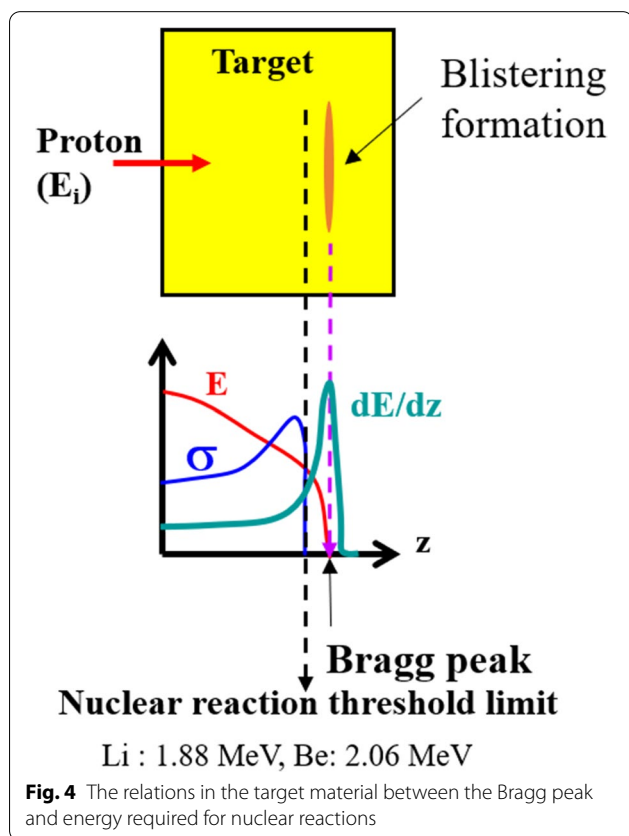
half-life of 53 days. Therefore, for a high beam power irradiation of, for instance, a beam with an energy of 2.3 MeV and a current of 30 mA, the resulting high radioactivity of the lithium target is currently the main issue for lithium-based BNCT facilities. The red dots in Fig. 3 mark the proton beam energies in existing BNCT facilities for lithium and beryllium targets. To provide the required

epithermal neutron flux, the proton beam currents range from 1 to 30 mA (on average) for various proton beam energies. As will be discussed in the next section, a low-energy (2.1~2.5 MeV) accelerator facility using a lithium target needs a current of 10 to 30 mA, a medium-energy accelerator needs 20 mA for 5 MeV and 2 mA for 8 to 10 MeV, and a high-energy accelerator (30 MeV) needs only 1 mA. Although the low-energy accelerator has the advantage of being small in size, the high-beam current operation could be a major hurdle to overcome in terms of thermal and radioactive issues coming from the lithium target, while the medium-energy accelerator using a beryllium target needs only one tenth of the required beam current of the low-energy accelerator and without any serious target thermal or radioactive issues.

In the p-Be reaction, a higher neutron yield is produced if the proton beam energy is higher than 8 MeV, and the neutron yield increases gradually with the proton kinetic energy. Therefore, the proton energy used for A-BNCT with a beryllium target is usually around 8–30 MeV. Even though the higher proton beam energy generates more intense neutrons, it also results in higher radioactivity around the target which is undesirable in a hospital setting. Besides, even with a beryllium target, a ${}^9\text{Be}(p,t){}^7\text{Be}$ reaction is opened for tritium and ${}^7\text{Be}$ production if the proton energy is more than 13.4 MeV [14]. However, beryllium is much easier to handle than lithium and its melting point is 1287 °C, although it is toxic when it becomes an oxidized powder. Of course, tritium production with a lithium target is also an issue that has to be managed even with a small amount of tritium.

2.3 Target thickness

As an incident particle penetrates the target, the kinetic energy of the particle decreases until it finally stops. The location where the particle stops is called the “Bragg peak.” With a proton beam, the material starts a “blistering” formation when the hydrogen concentration at a layer of Bragg peak position reaches a threshold limit

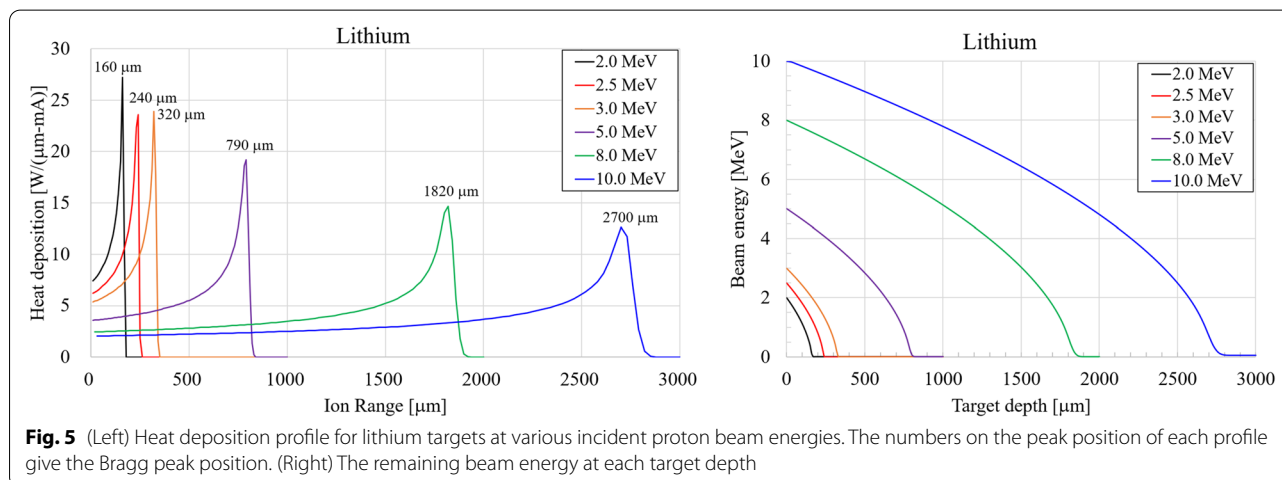


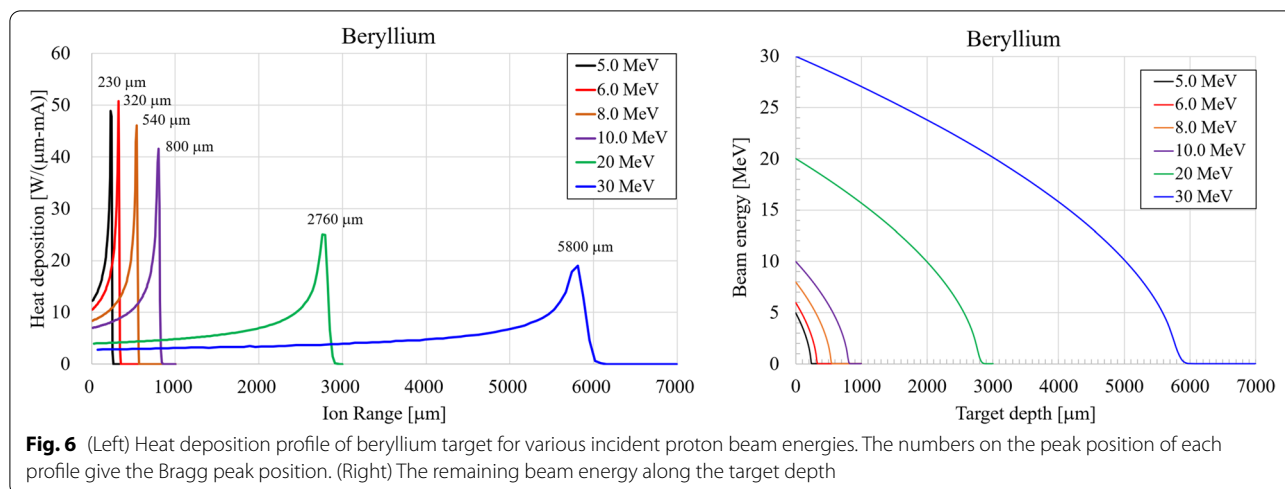
which depends on the material property [15]. This causes hydrogen embrittlement in a layered manner, and eventually hydrogen gas inflates into bubbles throughout the embrittled layer. It is well known that a thick beryllium target can be destroyed in a very short time because of hydrogen embrittlement. Figure 4 shows the concept. To avoid hydrogen embrittlement inside the target, the target structure is made with a backing material that has a high hydrogen diffusion coefficient and thereby a higher blistering threshold limit to increase the target lifetime. So, the target thickness should be thinned sufficiently to put the Bragg peak outside the target to protect the target, yet as thick as possible to maximize neutron production.

Figures 5 and 6 show the heat deposition profile and the remaining kinetic energy of the proton beam as a function of the penetration depth into the lithium and beryllium targets for various incident proton beam energies. These curves were calculated using the SRIM code which is a software package for calculating the stopping and the range of ions in a matter [16]. For the 10 MeV and beryllium target case used at DM A-BNCT, a target thickness of 0.7 mm is where the beam energy reduces to the nuclear reaction threshold limit and so is sufficient for neutron production while avoiding blistering of the beryllium target. For a lithium target and 2.5 MeV beam energy, a target thickness of 0.1 mm is good enough.

2.4 Survey of accelerators for BNCT

There are two types of accelerators used for BNCT around the world: the electrostatic (ES) accelerator and the radio-frequency (RF) accelerator. The principle of the ES accelerator is that the ions are accelerated by an electric field generated by a static electric potential applied between a terminal and a ground electrode. The principle of an RF accelerator is that ions are accelerated by





the electromagnetic energy in an electric field working at radio frequencies.

For an ES accelerator, there are also two different types depending on the technology for generating the high voltage. The first type is the Tandem accelerator using a conventional voltage multiplier. It accelerates negative ions first from one side at ground potential up to a gas chamber at a high positive potential, then the negative ions are converted to the positive ions by electron stripping. The positive ions are then accelerated back down to the ground side. Therefore, the beam energy is doubled in a relatively compact size. Thus, this is a good candidate for the A-BNCT source. The second ES type is a single-stage accelerator using solid-state inverter technology. This type requires a very large insulation tank to accommodate many inverter modules and a motor generator supplying AC power to each inverter module and an insulated belt.

For an RF accelerator, there are again two types: the linear accelerator (linac) and the cyclotron. There are two main components to the linac; a radio frequency quadrupole (RFQ) functions as a low-energy accelerator and a drift tube linac (DTL) is used for high-energy acceleration. Both the RFQ and DTL use a resonating cavity to hold the acceleration electric field coming from a high-power RF supply. Instead of a continuous flow of protons, an RF linac accelerates proton pulses in phase with the driving RF frequency.

The RFQ linac was invented by two Russian scientists, Kapchinskii and Teplyakov in 1969 [17]. It became popular around the world in the 1970s after a successful design method was established by the Los Alamos National Laboratory [18]. The RFQ linac bunches the DC input beam and also accelerates the bunched beam at the same time. Also, an RFQ linac can focus the beam by crafting

an electric quadrupole field generated internally with four electrodes called vanes. The vane surface is “modulated” within the period of $\beta\lambda/2$ to generate the longitudinal electric field needed for particle acceleration. Here, β is the particle velocity normalized to the speed of the light, and λ is the free space wavelength of operating RF frequency. The RFQ is a very popular linac for accelerating a DC beam from an ion source. Conversely, the DTL linac accelerates only an already bunched beam, usually coming from an RFQ linac. The DTL linac was invented by Alvarez [19, 20], and it became the most common proton accelerator. The DTL linac is a cylindrical cavity and its resonating mode is TM_{010} (zero modes of the two components of the azimuthal magnetic field and longitudinal electric field). Small cylinders called drift tubes (DT) along the cavity axis are installed to accelerate the particles along the cavity axis. The RF electric field generated in the gap between adjacent DTs changes its direction every half period of the RF cycle; thus, the particles see the same acceleration RF phase at every gap. For this, the length between adjacent DT centers is set to $\beta\lambda$. More details about the acceleration principle and characteristics of RFQ and DTL linacs can be found in the reference [21].

The cyclotron is a well-known accelerator type invented by Lawrence [22], and it eventually has become popular for the production of radioisotopes for medical applications. The moving particle in a circular motion under the uniform magnetic field undergoes an acceleration by the RF electric field between the “Dee” gap between semi-shaped hollow electrodes. Under a constant magnetic field, each turn period is also constant and does not depend on the particle velocity. Instead, the radius of the circular motion increases with particle velocity, and the particles spiral out. In Japan, a 30-MeV and 1-mA

cyclotron has been used for an A-BNCT neutron source, “C-BENS” (cyclotron-based epithermal neutron source). C-BENS was in fact the first A-BNCT in the world. For more detailed introductions to the ES and RF accelerators used for A-BNCT please refer to [14].

For an ES accelerator, the present high-voltage insulation technology limits the beam energy to a maximum of 2.5 MeV for high currents. The operating beam current ranges from 10 to 30 mA depending on the beam energy. Most of the A-BNCT facilities using lithium targets use an ES accelerator since they only need low energy around the resonance peak of the p-Li reaction. But, the BNCT facility at the National Cancer Center (NCC) in Japan uses an RF accelerator with a 2.5 MeV, 20 mA single RFQ and the lithium target [23]. At energies less than about 3 MeV, various facilities with ES accelerators have been constructed and many are under commissioning. All facilities using ES accelerator except in Argentina use lithium targets. At energies higher than 3 MeV, most A-BNCT facilities use an RF accelerator and beryllium target. Diverse beam energies and beam currents have been tried. The first A-BNCT was C-BENS (cyclotron-based epithermal neutron source) using a cyclotron accelerator and beryllium target at Kyoto University in Japan [24]. The cyclotron energy is 30 MeV and 1 mA. The protons at this energy require a very thick (~5 mm) beryllium target to generate enough neutron production based on Eq. (1). Owing to the large thickness, the target itself can be a compound structured material able to sustain the pressurized water layer placed just behind the target. Thus, most of the protons stop in the water layer preventing blistering inside the beryllium target. Since C-BENS is designed to treat deep-seated tumors, the resulting fast neutron contamination level is higher than the IAEA recommended value. C-BENS has been providing patient treatment in hospitals in Japan since 2020 (<http://www.sthg-jp.com/motion.asp?siteid=100511&menuid=10491&lqid=1>, <https://www.ompu.ac.jp/kbmc/index.html>). C-BENS was the first commercialized A-BNCT in Japan. A few other A-BNCT facilities using an RF linac and beryllium target are under development with beam commissioning and pre-clinical tests. Tsukuba University (iBNCT) in Japan using RFQ and DTL linacs is at the basic BNCT research stage conducting pre-clinical tests [25]. The beam energy is 8 MeV, and the designed current is 10 mA on average. In Italy, an A-BNCT facility is in planning based on a single 5-MeV RFQ linac [26]. The RFQ was developed in the Laboratori Nazionali di Legnaro (LNL) many years ago [27] and has a beam current of 30 mA. In Korea, DawonMedax constructed an A-BNCT facility based on an RFQ and DTL linac in 2018 and human clinical trials will begin soon in 2022. The beam energy of the DM A-BNCT

accelerator is 10 MeV and the designed beam current on average is 8 mA. But, the operating nominal beam current is only 2 mA which still produces a sufficient epithermal neutron intensity at the IAEA-recommended level for the clinical trials. This excellent performance is attributed to the high efficiency of the beam-shaping assembly. More details on the status and information about A-BNCT facilities are found in the reference [28]. Table 2 shows the list of A-BNCT facilities around the world as updated in Table 2 in reference [28].

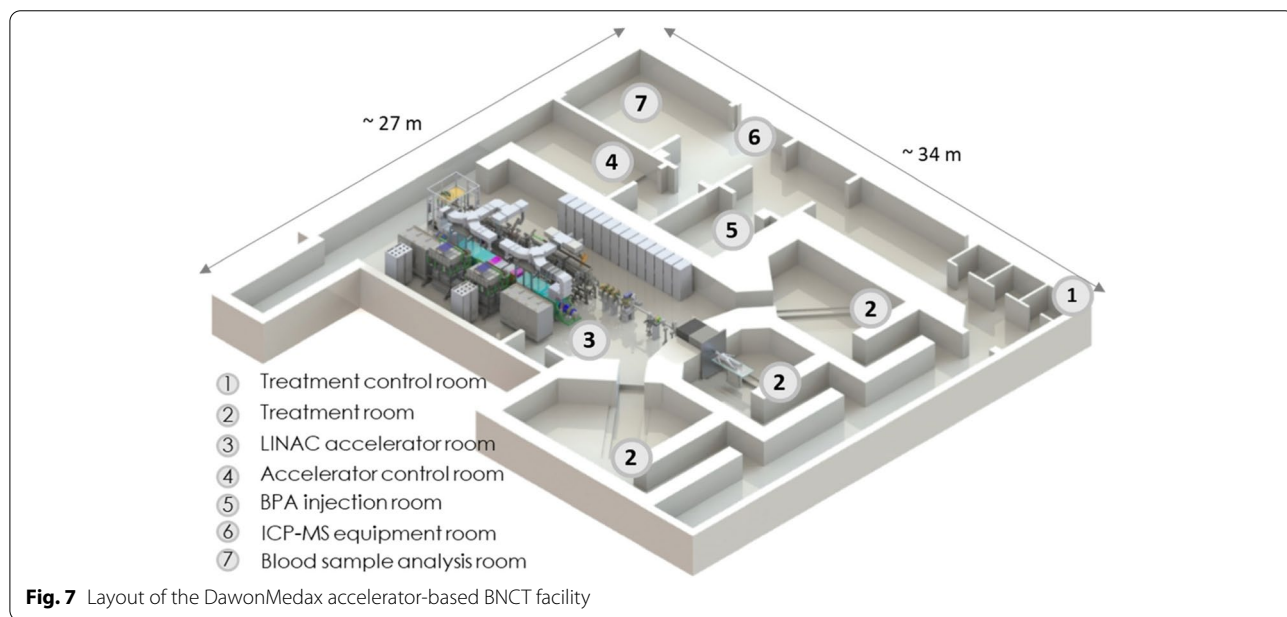
3 Development of A-BNCT in Korea

3.1 Facility design and layout

The first A-BNCT facility in Korea was LENS10 developed by the DawonMedax company [35, 36]. The acronym LENS10 came from its being a “10-MeV linac-based epithermal neutron source.” Figure 7 shows the layout of the DM A-BNCT facility with LENS10 using a beryllium target. The decision between lithium and beryllium targets was based on the insights of the previous discussion; thus, the beryllium target was chosen after putting weight on the aspects of target radioactivity and cooling. The goal of the DM A-BNCT facility was to create a compact BNCT facility that could be adopted by hospitals to provide cancer therapy. Therefore, the final proton beam energy was limited to 10 MeV to minimize the radioactivity of the material surrounding the target. The facility consists of an accelerator room, three treatment rooms, and a treatment control room. The dimensions of the facility’s base floor plan are 27 m x 34 m and 5 m high. The neutron source is placed in a radiation-shielded room as shown in Fig. 7. The treatment rooms and accelerator control room are on the same floor. The radiation shielding wall is made of concrete. The wall thickness surrounding the accelerator room is 1 m, and the wall thickness between the accelerator room and treatment rooms is about 2 m. The beam shaping assembly (BSA) forming the neutron moderator system is placed in the inner concrete wall between the accelerator and treatment rooms to reduce the size of the neutron and γ -ray shield structure. The treatment rooms and accelerator room are maintained at a negative air pressure for radiation safety. Also, the inner concrete walls of the treatment room are covered with boronated plastic and lead plates for radiation protection by capturing stray neutrons, thereby preventing more neutron scattering. It is necessary not only for shielding neutrons and γ -rays but also for the reduction of neutron activation of air, walls, and patients. The neutron activation of air in the treatment room is mainly focused on the neutron activation of argon, in which the β -emitter Ar-41 with a half-life of about 109 min is produced, in facility radiation safety

Table 2 List of A-BNCT facilities around the world

Facility name	Accelerator	Target	Incident particle energy (MeV)	Designed current (mA)	Present current (mA)	Status
Kyoto Univ. (Japan)	Cyclotron	Be	p:30	1	1	Treatment (commercialized)
Southern Tohoku Hosp. (Japan)	Cyclotron	Be	p:30	1	1	Treatment (commercialized)
Kansai BNCT Medical Center (Japan)	Cyclotron	Be	p:30	1	1	Treatment (commercialized)
Tsukuba Univ. (Japan)	Linac	Be	p:8	10	< 2	Pre-clinical test
DM A-BNCT (DawonMedax, Korea)	Linac	Be	p:10	8	2	Starting clinical trial
Legnaro INFN (Italy)	Linac	Be	p:5	30	-	Developing
National Cancer Center (Japan)	Linac (RFQ)	solid Li	p:2.5	20	12	Clinical trial
Edogawa Hospital BNCT Center (Japan)	Linac	solid Li	p:2.5	20	-	Constructing
Nagoya Univ. (Japan)	Electrostatic	solid Li	p:2.8	15	1 [29]	Commissioning
Budker Inst. Nucl. Phys (Russia)	Electrostatic	solid Li	p:2.0	10	3	In-vivo test [30]
Helsinki Univ. Central Hospital (Finland)	Electrostatic	solid Li	p:2.3	30	30	Commissioning [31]
Xiamen BNCT Center (China)	Electrostatic	solid Li	p:2.5	10	4 (at 2.3 MeV)	Pre-clinical test (https://en.neuboron.com/news/294.html)
CNEA (Argentina)	Electrostatic	Be, 13C	p,d:1.4	30	<1	Constructing
Granada (Spain)	Electrostatic	solid Li	p:2.1	30	-	Planning [32, 33]
SARAF (Israel)	Linac (RFQ + HWR)	Liquid-Li	p: 2.5	20	2	Developing [34]



regulation. The DM A-BNCT facility evaluated that the argon activation level after the 1h neutron irradiation is less than the maximum regulated level (5×10^4 Bg/ m^3) by the Korea Nuclear Safety authority. The neutron activation of concrete walls around the BSA is regularly monitored. In fact, whereas the neutron activation of

the patients is often overlooked, it is very important to point out the safety of those who contact patients after the treatment. The residual specific activities of the patients could be soft tissue and urine. Therefore, the need for special restrooms to store urine is being discussed before the clinical trials even with borated

shielding walls surrounding the treatment room mentioned above.

The facility is equipped with dosimeters, neutron and γ -ray radiation monitoring system (RMS), neutron flux monitors, CCD cameras in the treatment rooms and accelerator room, high-purity germanium (HPGe) γ -ray detector, ICP-MS equipment for boron concentration measurement in the blood samples, etc. Water pumps and various electrical utility infrastructures are located on the first floor but are not shown in Fig. 7.

3.2 Linac

Figure 8 shows the layout of the proton linac. The total length from the ion source to the beryllium target is about 20 m. The linac consists of the ion source, low-energy beam transport (LEBT), 3-m-long radio frequency quadrupole (RFQ), 5-m-long drift tube linac (DTL), and beam transport line (BTL). The beryllium target for neutron production by the ${}^9\text{Be}(p,n){}^9\text{B}$ nuclear reaction is placed inside the moderator and shielding structure, which together is called the “beam shaping assembly (BSA).” The BSA is installed inside the wall between the accelerator room and treatment rooms.

The 50 keV primary proton beam extracted from the ion source is transported by a LEBT equipped with two electromagnetic solenoids to focus the proton beam at the RFQ inlet. The focused and matched proton beam is then accelerated by the RFQ up to 3 MeV, and then, it is accelerated further up to 10 MeV by the DTL which is almost directly connected to the RFQ. The RFQ and DTL

linacs are designed to operate at an RF frequency of 352 MHz. The designed maximum peak current of the beam pulse is 40 mA.

While the linac is capable of a peak beam current of 40 mA at a 20% duty factor, the design is optimized to be operated with an average current of 8 mA. A pulse duration of 1.7 ms and repetition rate (PRR) of up to 120 Hz determine the 20% duty factor. Because of the high epithermal neutron conversion efficiency of the BSA, the IAEA-recommended epithermal neutron flux can be comfortably supplied even at the average beam current of only 2 mA. However, even that is still high enough that there could be RF breakdown issues in the RFQ and DTL linacs if the lower peak current necessitates a higher duty factor in the RF power supplied. A lower peak current is preferable in reducing the possibility of beam loss.

3.2.1 Ion source

The duo-plasmatron ion source is a plasma-based ion source that generates protons by an arc discharge in hydrogen gas. A low-pressure arc discharge in the gas to be ionized is electrostatically constricted by a funnel-shaped intermediate electrode placed between the electron-emitting cathode (tungsten filament) and the anode. A strong axial magnetic field between the intermediate electrode and the anode further constricts the discharge to a narrow plasma beam along the axis of the exit aperture. Figure 9 shows the inner structure of the duo-plasmatron ion source. It features extraction of a high current proton beam with low emittance

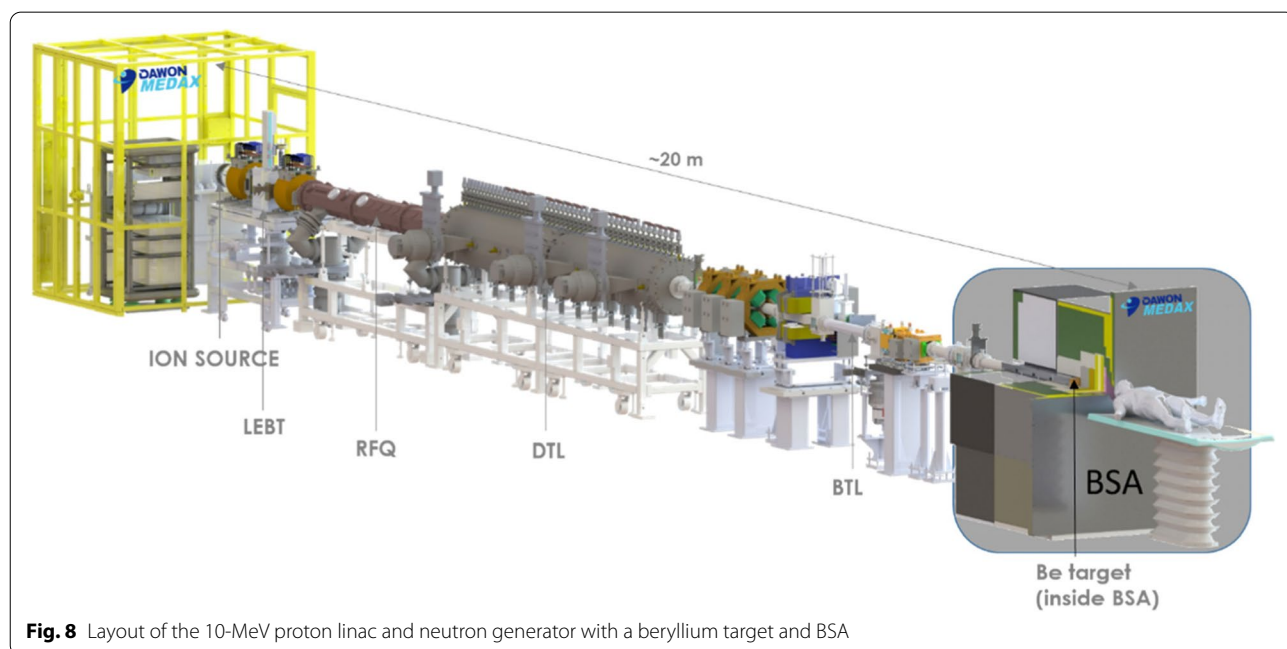
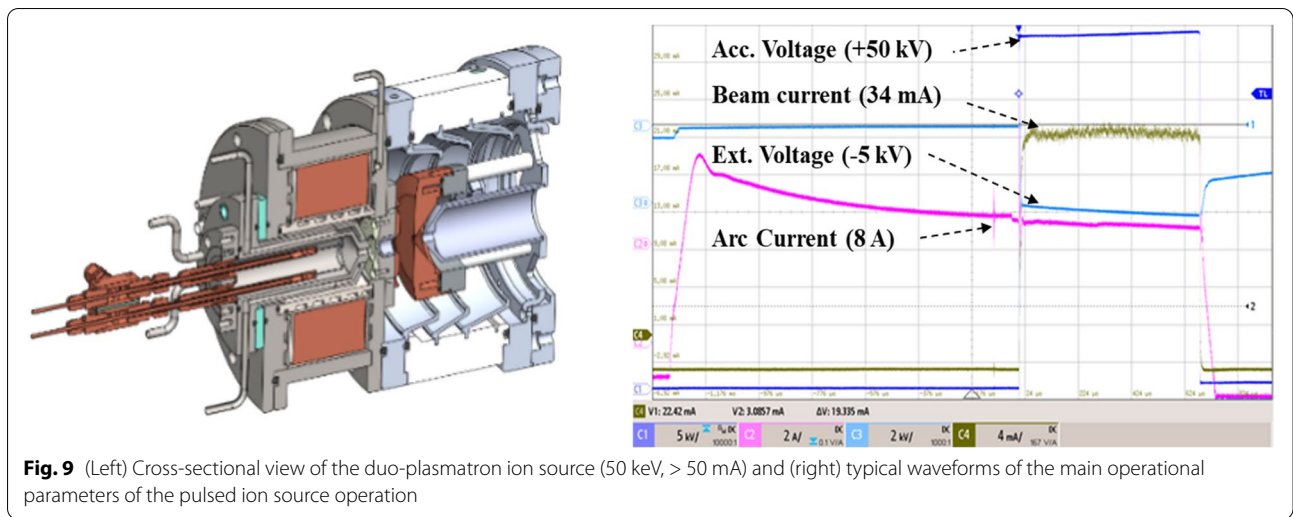


Fig. 8 Layout of the 10-MeV proton linac and neutron generator with a beryllium target and BSA

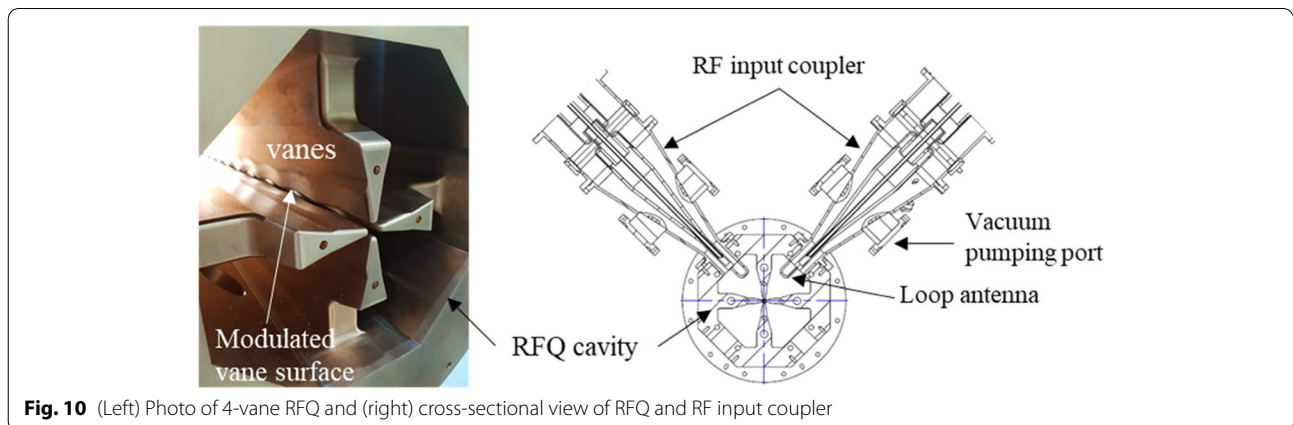


(< 0.2 pi-mm-mrad in normalized RMS units). For BNCT treatment, a highly stable arc plasma discharge is required for a stable proton beam extraction at high currents (> 50 mA), since the requirement is for the irradiation of constant neutron flux. To meet this requirement, we used a solid-state pulse modulator with precise control of an inverter-based capacitor charging power supply. The solid-state pulse modulator system provides a high voltage (50 kV) for the beam extraction with high stability (< ±1%). The arc discharge current is actively controlled to extract a constant peak current in the beam pulse. This has the effect of reducing the evaporated tungsten contamination on the intermediate electrode. The ion source is shown in Fig. 9 along with waveforms of an arc plasma discharge current with a pulse duration of 2 ms, at a 50-kV acceleration voltage, and a negative 5-kV extraction voltage. The extraction voltage turns on at 1.3 ms after the arc plasma discharge. The beam current is measured by an AC current transformer (ACCT) at the entrance of the RFQ.

3.2.2 RFQ linac

The RFQ linac is made of oxygen-free high conductivity copper. The RFQ is designed to have a 4-vane structure with inner and outer diameters of 19 cm and 33.4 cm, respectively. Figure 10 shows the 4-vane RFQ structure and a cross-sectional view of the RFQ cavity and RF input coupler. The RFQ consists of three segments of 1-m length each. The input beam energy is 50 keV, and the output is 3 MeV. The RF power supply is designed to provide 450 kW in total; this accounts for copper wall loss power plus the beam power. More details on the RFQ physics design are reported in reference [37].

When tasked with providing a very stable beam at a high average RF power, the RFQ can be difficult to operate without RF breakdown. There is a strong relationship between the stability of the RF input power and interactions between the cavity discharge and/or the input coupler's discharge. Once an RF breakdown begins, RF power no longer feeds into the cavity due to impedance mismatching, and consequently, the power is reflected



and it can be monitored by a directional coupler. To protect the RFQ cavity and avoid more immediate RF breakdowns, the next RF pulse is applied after about a 0.5 to 1 s delay with the beam turned off. A slight temperature drop in the RFQ cavity wall causes a corresponding increase in the resonant frequency. The amount of the shift of the resonant frequency at the next RF pulse determines the recovery time in the RFQ cavity resonance frequency. During this recovery phase, no proton beam is supplied or accelerated. In medical applications, the duration of the beam-off time due to any fault during the patient treatment is called “beam downtime.” To reduce RF breakdowns, an oversized vacuum pumping system composed of turbomolecular pumps and cryosorption pumps is installed on the RFQ tank. Also, additional vacuum pumping to the RF input couplers helped mitigate frequent RF breakdowns inside the input couplers. To further minimize the accumulated beam downtime, a fast recovery is also essential. To this end, cooling water channels were modified to increase the water flow rate and reduce the temperature change of the RFQ cavity during the RF breakdown recovery phase. For fast recovery of RF stability, it is important that the resistance to a thermal energy transfer from the cavity body to the cooling water is sufficiently small and that therefore the temperature change of the RFQ cavity during the RF breakdown period is reduced by the increased cooling water flow. Also, feedback control of the resonance frequency in the low-level RF (LLRF) system is implemented with reflected power monitoring.

3.2.3 DTL linac

The DTL linac is designed to be of the Alvarez-type with 48 drift tubes (DT). The bore diameter of the DT is 20 mm. The tank is made of stainless steel, copper-plated on the inner surface. The tank’s inner and outer diameters

are 48 cm and 58 cm, respectively. The length of the DTL is about 4.8 m. Inside the DTs, there are quadrupole electromagnets to focus the beam during the acceleration through the DTL tank. The focusing lattice is assembled with a DDF (defocusing-defocusing-focusing-focusing) arrangement. The maximum field gradient of the quadrupole magnet is 50 T/m. Figure 11 shows the inner structure of the DTL linac and a beam trace simulation using the TraceWin code [38] for the RFQ output beam. The first 10 DT electromagnets are used for beam matching. The vacuum pumping system consists of three turbomolecular pumps. The designed RF power is 700 kW including the beam power. The input beam energy and output beam energies are 3 MeV and 10 MeV, respectively. The DTL linac is not subject to RF stability problems due to routine RF breakdown.

3.2.4 Beam transport line (BTL)

The main role of the BTL is naturally transporting the beam to the targets. Each of the three treatment rooms is 45° from its neighbor. The BTL length is about 6.5 m. The beam is focused on the target using only a single triplet quadrupole magnet system placed near the exit of the DTL. Other components of the BTL are steering magnets, beam profile monitors, an ACCT for beam current measurement, a vacuum pump, and fast-beam scanning magnets. Figure 12 shows the layout of the BTL showing from the DTL exit to the beryllium target.

3.2.5 RF system

The DM A-BNCT proton accelerator has two separate RF systems for flexibility of operation and control of the RFQ and DTL linacs. Each RF system is equipped with a 352 MHz klystron made by the Thales Group and a low-level RF (LLRF) system. The maximum peak RF output power of each klystron is 1.5 MW, and the maximum

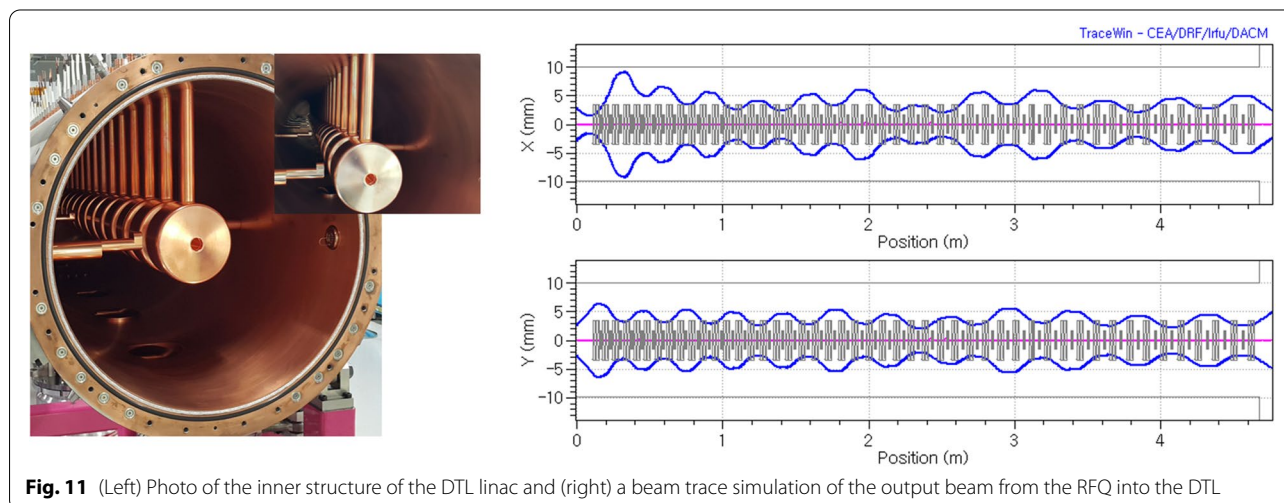


Fig. 11 (Left) Photo of the inner structure of the DTL linac and (right) a beam trace simulation of the output beam from the RFQ into the DTL

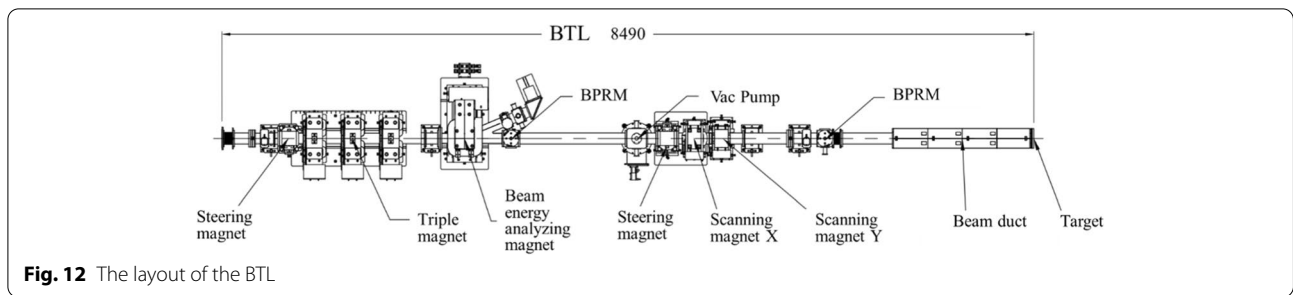


Fig. 12 The layout of the BTL

average power is 300 kW. Because of the strong dependence of accelerator performance on the stability of the RF power and phase between pulses and even within each pulse, a high-precision solid-state switching technology was designed into the modulator system and used for operating the klystrons. The developed modulator has a very high pulse-to-pulse stability that is less than $\pm 0.1\%$ at a maximum high voltage of 90 kV with a pulse width of 1ms and a pulse repetition rate of 120Hz. The LLRF controls the amplitude and phase of the RF drive signal which is fed into the input cavity of the klystron. Also, there is a feedforward control of the RF output and phase compensation that can be applied if there is a high voltage drop in the modulator circuit for the pulse width longer than 0.5 ms. The modulator and LLRF system thus are also key components in the total RF linac system.

3.3 Linac operation performance

A neutron irradiation time longer than 45 min could be required to meet the required boron dose for brain tumors. Because of the constant concentration decay of the boron agent in the patient during the treatment, the

actual delivered treatment time must be within the 5% excess time of the planned treatment time. So, the proton linac should be operated stably. Except for RF breakdown events in the RFQ, this is usually not a problem. For each RF breakdown event, the beam pulse is turned off for 3 to 5 s depending on the RF breakdown situation. Figure 13 shows an example of a long operational run. In this run, several RF breakdown discharges occurred in the RFQ linac. Most of the breakdown discharges were recovered quickly, and the total beam-down time was about 2%. The RF breakdown discharge occurred at about a 0.1/min rate. We further note there are no RF breakdowns occurred in the DTL linac.

3.4 Neutron source system

3.4.1 Beryllium target

As noted previously, the target material for the DM A-BNCT is beryllium. Neutrons are produced by the ${}^9\text{Be}(p,n){}^9\text{B}$ reaction. For a beam with an energy of 10 MeV and a current of 2 mA, the neutron yield delivered near the target is in the order of 4×10^{13} n/s, and this is from a Monte Carlo code simulation. Currently, the

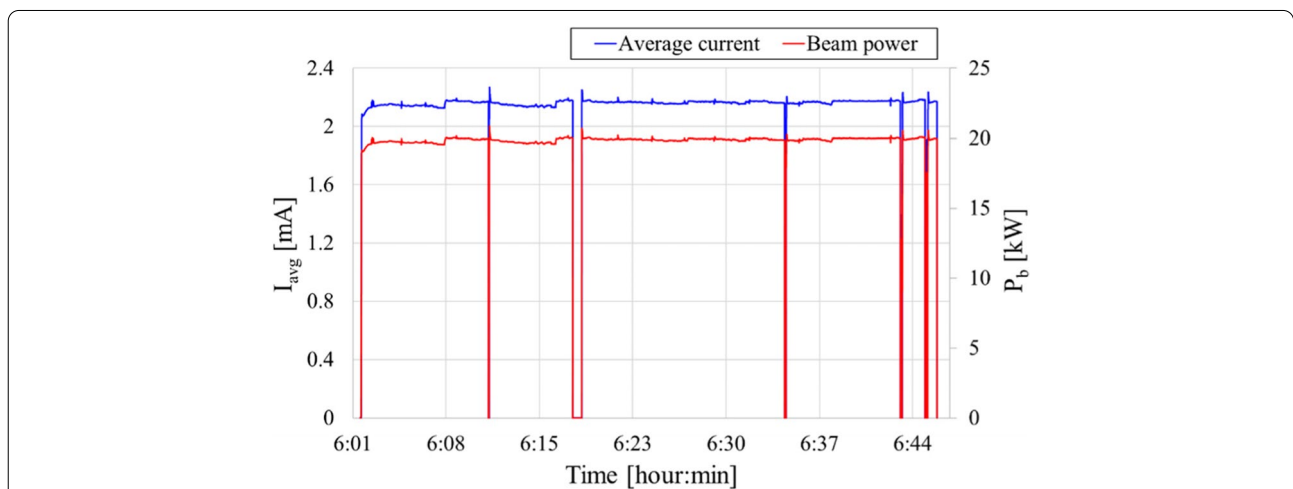


Fig. 13 The long-run operation data shown are the average beam current (I_{avg}) and the calorimetric beam power measurement (P_{beam}). RF breakdown discharges are indicated by the vertical lines in the average beam current (blue line) and hence the calorimetric power measurement (red line)

beryllium target thickness is chosen to be 1 mm which is thicker than the “Bragg peak: depth; thus, all protons stop inside the beryllium target. Because the Bragg peak depth is 0.8 mm for a 10 MeV incident proton beam energy, the lifetime of the 1-mm-thick beryllium target is therefore at risk if the hydrogen gas density rises above the threshold where “blisters” start to occur on the surface of the target. Depending on the proton beam size and current, this blistering could happen within a range of a few or tens of hours. Therefore, to increase the lifetime of the beryllium against blistering, the target thickness will be reduced to 0.7 mm. Such a reduced thickness would be sufficient to slow down a proton beam with 10 MeV incident energy to as low as 2 MeV on the target exit which is the threshold energy for the p-Be reaction. Further vanadium material will be bonded behind the beryllium so that the proton beam stops inside the vanadium. The blistering threshold of vanadium is about 10 times higher than that of beryllium [15]. The current neutron-generating target is a 1-mm-thick beryllium target brazed to a copper heat sink block into which a cooling water channel has been machined. The development work on a longer life target combining a thinner beryllium layer bonded with a vanadium backing material is underway and will be tested shortly to ensure the expected long lifetime can be achieved.

To reduce the number of neutrons and γ radiation in the backward direction, the proton beam duct line connected to the beryllium target is restricted to 10 cm in width and 10 cm in height. The beryllium target is made to be the same size as the proton beam duct. Here, difficulty in removing the high heat flux from the bombarding proton beam presents itself. The incident proton beam pulse profile is basically a Gaussian with an RMS radius of 2 cm and a peak beam power density of 20 kW/cm² for each single beam pulse. The heat flux would be very large if the beam were stationary and constantly bombarded at the same position. To mitigate this, a beam scanning system is implemented to spread the heat flux over the target. The water-cooling structure on the copper backplate is specially designed to provide a high thermal transfer coefficient through a turbulent flow caused by a high-water flow speed. Figure 14 shows a schematic drawing of the beryllium target assembly. The time structure of the proton beam pulse has a duration of 0.66 ms and a repetition rate (PRR) of 120 Hz. In the beam scanning system, the beam is controlled to rotate around the target center. Each step of beam movement is preset in the scanning control algorithm, and the beam deflection from the scanning electromagnets is synchronized with the beam pulse repetition rate. This scanning method is commonly called “wobbling.” From a time-dependent

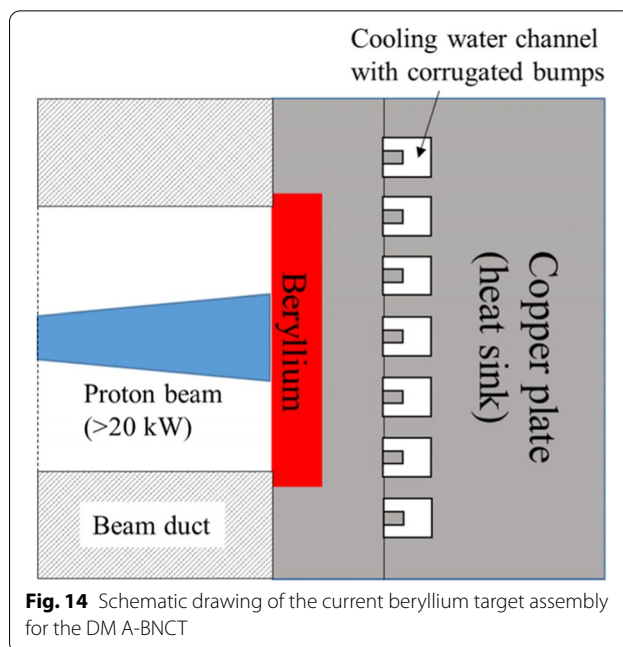


Fig. 14 Schematic drawing of the current beryllium target assembly for the DM A-BNCT

thermal analysis, the temperature increment on the beryllium surface rises instantaneously by up to 30 °C whenever a single pulse hits the target. Eventually, the steady-state temperature of the beryllium target reaches a saturation level of 140 °C.

3.4.2 Beam shaping assembly (BSA)

BSA design The beam shaping assembly (BSA) is another essential component in A-BNCT as it functions to convert incident fast neutrons with an average energy of 2.8 MeV coming from the beryllium target into a beam of epithermal neutrons with characteristics suitable for clinical applications. The BSA was designed using the Monte Carlo N-particle transport (MCNP6) code [39]. The BSA consists of a magnesium fluoride (MgF₂) moderator, a composite reflector of aluminum near the target and lead blocks, and filters for fast neutrons, thermal neutrons, and γ radiation. A high-density block of polyethylene (HDPE) on the upstream side of the BSA attenuates neutrons reflected from the target. The BSA is mounted on a concrete block, which is itself on a rail system to facilitate access for target replacement. A borated polyethylene sheet surrounds the BSA to shield thermal neutrons. Figure 15 presents a cross-sectional view of the DM A-BNCT BSA.

Collimator The DM A-BNCT BSA is designed to handle the mainly epithermal energy components of the neutrons that pass through the moderator blocks. The epithermal neutrons are centralized in the beam

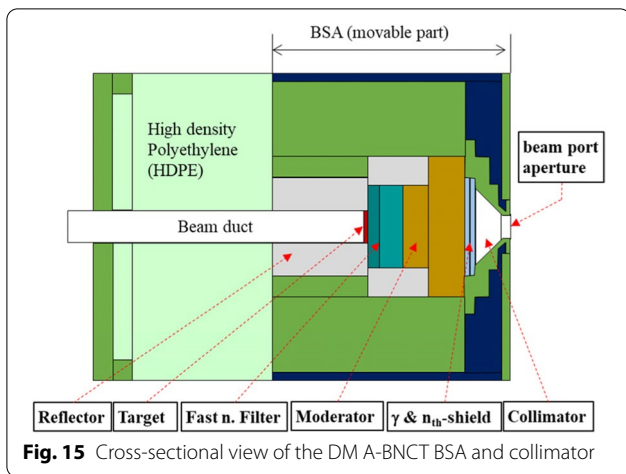


Fig. 15 Cross-sectional view of the DM A-BNCT BSA and collimator

aperture using a collimator installed behind the thermal neutron and γ -ray filters. The collimator mainly consists of lead and borated polyethylene (BPE) blocks. Neutron beams are delivered to the beam aperture at the end of the collimator by passing through a cylindrical cone-shaped air beamline as seen in Fig. 15. The cone angle and length are optimized to have maximum epithermal neutron flux at the beam aperture exit. The beam aperture diameter is 12 cm.

Neutron beam characteristics The MCNP simulation shows an epithermal neutron flux of 1.03×10^9 n/cm²s at the BSA beam port when the proton beam average current is 2 mA and an energy of 10 MeV. This gives a high ratio of epithermal neutron flux to proton beam power: 5×10^7 n/cm²s/kW. The remaining undesired contributions of thermal neutrons, fast neutrons, and γ radiation are all acceptably small: $\Phi_{th}/\Phi_{epi} = 0.003$, $D_{fast}/\Phi_{epi} = 3.3 \times 10^{-13}$ Gy-cm², $D_{\gamma}/\Phi_{epi} = 0.9 \times 10^{-13}$ Gy-cm². All

neutron beam parameters at the beam port meet the IAEA-recommended values except that the fast neutron dose ratio is slightly higher than the IAEA-recommended value ($\leq 2.0 \times 10^{-13}$ Gy-cm²). As a new figure of merit (FOM) to aid in BSA design improvements, we define the epithermal neutron conversion efficiency to be: $\Phi_{epi}/Y = 2.5 \times 10^{-5}$ cm⁻². Here, Y is the total neutron yield at the beryllium target integrating over solid angle and energy. Figure 16 shows the neutron energy spectra at selected positions from the target to the beam aperture exit and a lateral profile of the epithermal neutron flux at selected longitudinal locations. At the target, the neutron energy spectrum is dominated by high-energy neutrons. The neutron energy at the peak intensity is 1 MeV, and the average neutron energy is 2.5 MeV. The high-energy neutrons are filtered by fast neutron filters with no change of neutron intensities below 100 keV. A more efficient moderator is needed to further slow down high-energy neutrons within a shorter distance and to avoid high radioactivity of the filter material as well. However, the low-energy neutrons also slow down after passing through the moderator. The γ -ray filter made of bismuth (Bi) slightly attenuates the neutron intensity. For the lateral profile of epithermal neutron flux at the beam port, as shown in Fig. 16b, the flux decreases by about 30% within the beam aperture exit. The peak value of the epithermal neutron flux at the center of the beam aperture exit decreases by about 10% when the distance from the beam aperture exit is increased by 1 cm.

Figure 17 presents the lateral flux profiles of each component at the BSA port. The epithermal neutron flux is reduced by about 2 orders of magnitude within the first 15 cm from the center axis. In the inner field region within the beam port, the fast neutron flux is about

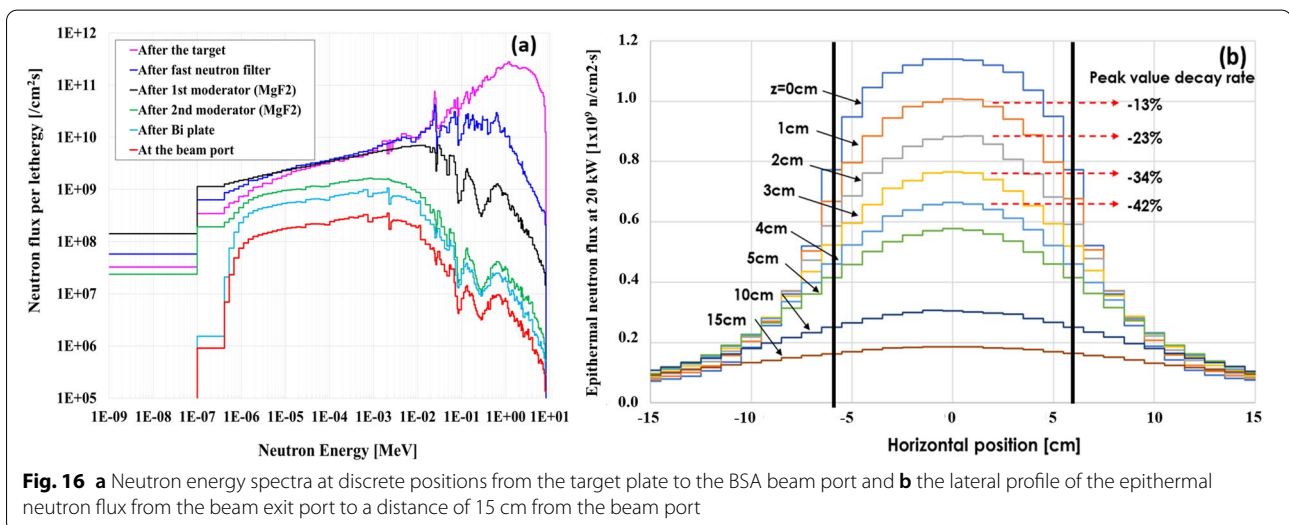
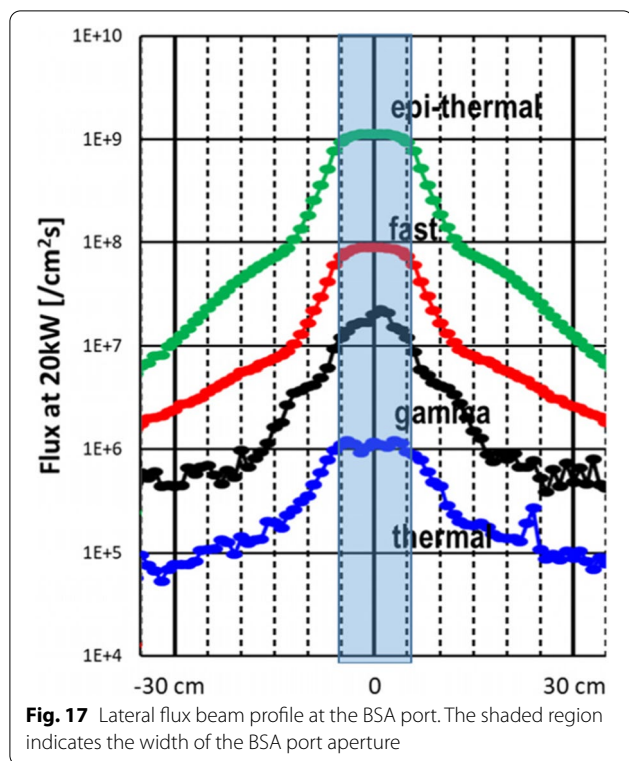


Fig. 16 **a** Neutron energy spectra at discrete positions from the target plate to the BSA beam port and **b** the lateral profile of the epithermal neutron flux from the beam exit port to a distance of 15 cm from the beam port



one tenth of the epithermal neutron flux, the γ radiation is lower by 2 orders of magnitude, and the thermal neutron flux by 3 orders of magnitude. The γ radiation is well attenuated at safe margins throughout the entire irradiation area. To confirm the safety of the out-of-field region, the biological effects on the human body in the out-of-field region were studied. For this study, a water-filled polymethylmethacrylate (PMMA) phantom of the human body was used, placing BPA-treated CHO cells with ^{10}B 25 ppm at several positions corresponding to the head, neck, chest, abdomen, arm, pelvis, thigh, lower leg, and foot of the phantom [40]. The phantom is positioned with a neutron beam axis aligned to the center of the head. The irradiation neutron fluence was determined to have 13 Gy-Eq (allowed maximum limit of normal brain tissue) on the head CHO cell. Here, the unit of Gy-Eq is a newly defined quantity, a proxy for “dose equivalent,” given by the National Council for Radiological Protection (NCRP) using newly defined field-dependent RBE values for specific components [41]. Based on the evaluation of the dose at each position, all the equivalent doses are less than 2 Gy-Eq, which is the regulated limit to avoid skin damage [42]. The highest dose is observed at the neck with 1.238 Gy-Eq.

Considering the size and location of the tumor and organs at risk around the tumor, the installation of an

additional beam aperture at the beam port is being planned. The proper type of beam aperture used for clinical tests will be determined based on the treatment planning system.

Online beam monitor Online neutron beam-monitoring detectors using LiCAF scintillator detectors are placed inside the collimator. They view directly the epithermal beam. The accumulated treatment doses will be monitored during BNCT treatment, and the irradiation will be automatically terminated when the neutron fluence reported by the beam monitors reaches the planned fluence. For the accurate measurement of the neutron fluence, the LiCAF detector is managed by regular calibration against a gold foil activation measurement. This provides a more direct measurement of the delivered dose than relying on calibrated proton current data. It can be also used for monitoring the accelerator stability and any problem with the target as well.

In-phantom figures-of-merit The in-air neutron beam parameters are almost all in full compliance with the IAEA recommendations. In-phantom dose simulation has been performed to evaluate the clinical adequacy for BNCT treatments targeting a brain tumor with the DM A-BNCT parameters in the MCNP6 code and the Snyder head phantom model [43]. This model is a spherical shape consisting of the skin, skull, and brain volume and with tumors uniformly distributed in the brain. For dose calculation with the Snyder head phantom model, four dose components are used: (1) the first one is the fast neutron dose which is calculated from the interaction between the fast neutrons and hydrogen, (2) the second one is the thermal dose from the interaction between the thermal neutrons and nitrogen, (3) the third one is the boron dose from the thermal neutrons and ^{10}B , and (4) the last one is the γ dose contributed by the primary γ radiation from the BSA port and prompt γ radiation generated from neutron interactions above. For the boron dose, we used the ^{10}B concentration ratio of the tumor to normal tissue of 3.5, and a ^{10}B concentration in the tumor tissue of 65 ppm which is similar to many other BNCT studies have used [44–46]. More details of dose components in the human body are explained in the next section. Several figures of merit (FOM) have been used to characterize the quality of the beam, and the FOM itself is well defined in reference [33]. Here, the definition of each FOM is again explained; advantage depth (AD) is defined by the depth where the dose to the tumor equals the maximum dose to the normal tissue; advantage depth dose rate (ADDR) is defined by the maximum delivered dose rate to the normal tissue; treatable depth (TD) is defined by the depth where the tumor dose falls below

twice of the maximum dose to normal tissue; maximum treatment dose ratio (TR) is defined by the ratio of the maximum delivered dose rate to the tumor to normal tissue; treatment time (TT) is defined by the estimated time to reach the allowable dose of the peak dose to the healthy tissue, namely 12.5 Gy-Eq; and average treatment dose ratio (AR) is the ratio between the total tumor and normal tissue dose, each one integrated from the tissue surface to the AD. A higher TT means that a higher dose of tumor tissue is allowed. Figure 18 shows the depth dose profiles for a Snyder head phantom. AD is more or less 9 cm with an ADDR of 0.327 Gy-Eq/min with no consideration to the skin dose where a peak appears early in the normal tissue dose rate profile. TD is 7.2 cm. The TR and AR ratios reach values of 5.91 and 4.76, respectively. The maximum TT is approximately 38 min. Our TD reaches a similar depth as the reactor-based BNCT facilities [47]. Although AD is slightly less than the above reactor’s AD, the ADDR of 0.327 Gy-Eq/min in our case is better compared to 0.45 Gy/min at FiR-1 and 0.50 Gy/min at THOR. Therefore, the DM A-BNCT neutron beam is considered to provide a promising therapeutic effect for deep-seated brain tumors. The dose rate components in the brain tissue are also seen in Fig. 18 (right).

3.5 Dosimetry

Radiation dosimetry, as used in the fields of medical physics and radiation protection, is the calculation, measurement, and assessment of an ionizing radiation dose absorbed by an object, usually the human body. Although there is no international standard for BNCT neutron and γ -radiation dosimetry, the dosimetry is usually measured and assessed based on the recommendations published by the IAEA [10]. The main dose contributions in the human body can be divided into three general groups: the dose from thermal neutron reactions with nitrogen (D_N) and ^{10}B (D_B), the γ dose (D_γ), and the fast-neutron elastic and inelastic collisions with hydrogen nuclei (D_{fast}).

3.5.1 Method

Based on the IAEA recommendations, the neutron activation method is used for thermal neutron dosimetry and neutron energy spectrum. For fast neutron and γ -radiation dosimetry, the paired-ionization chamber method is used. The measurements are performed inside a water-filled rectangular phantom made of PMMA, 30 cm in width, 30 cm in height, and 30 cm in depth. The measured neutron fluence is weighted with the total kinetic energy released in materials (KERMA) factor [48] and an RBE factor to calculate the absorbed dose in each of the brain elements, including ^{10}B elements assumed to have a uniform density in the brain phantom. In addition, the LiCAF scintillator detector used for online epithermal neutron flux monitoring is calibrated by the neutron activation method.

3.5.2 Dosimetry results

Before dosimetry measurements, the neutron energy spectrum at the BSA beam port aperture is confirmed using the multi-foil activation method. The activated foils used are In, Cu, NaCl, Zn, Co, Mo, Sc, Zr, and Mn-Cu. Each foil has different neutron activation dependencies on neutron energy. The foils were installed in an array in front of the BSA beam port aperture, and the activation level was measured using an HPGe γ -ray detector. An unfolding procedure is used to determine the energy spectrum [49]. A comparison of the unfolded neutron spectrum against the MCNP simulation shows reasonable agreement within measurement uncertainties. Figure 19 shows the MCNP simulation calculated neutron energy spectrum and the multi-foil activation measured spectrum. With an agreement of $\pm 2\%$, we have confidence in using the multi-foil activation method to determine the BNCT neutron spectrum.

The nitrogen dose and ^{10}B dose are not measured directly, but are calculated from the thermal neutron flux measured with the neutron activation method. For the thermal neutron dose measurement (nitrogen and ^{10}B dose), neutron activation of a gold wire 0.5 mm in

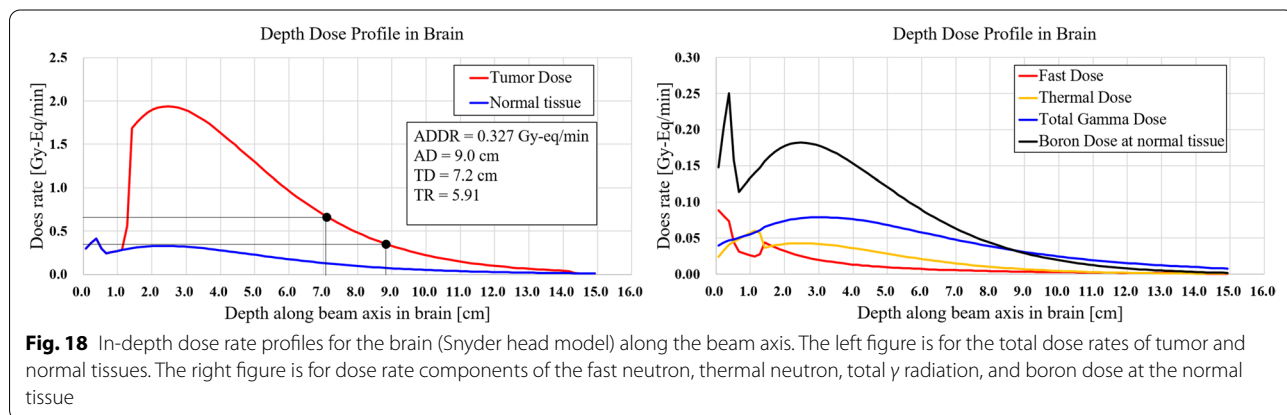


Fig. 18 In-depth dose rate profiles for the brain (Snyder head model) along the beam axis. The left figure is for the total dose rates of tumor and normal tissues. The right figure is for dose rate components of the fast neutron, thermal neutron, total γ radiation, and boron dose at the normal tissue

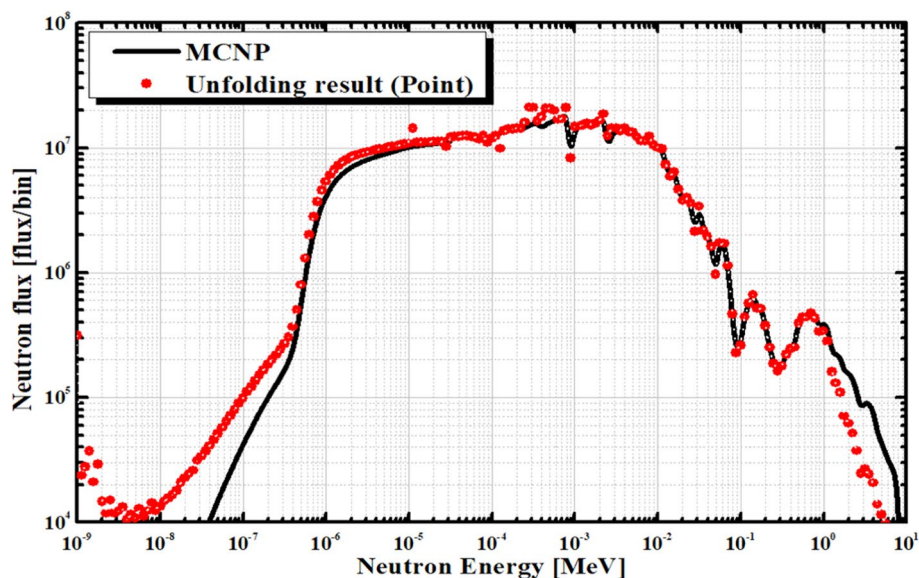


Fig. 19 Neutron energy spectrum as measured by multi-foil activation and unfolding compared with the MCNP simulation

diameter and 10 mm long placed on the central axis of the phantom is used. The gold wire has a high nuclear reaction rate with thermal neutrons. The paired ionization chamber method [48] for fast neutron beam dosimetry is the recommended method for direct measurements of the total dose of neutron and γ radiation in BNCT. The total dose is measured with a tissue-equivalent (TE) plastic (A150) chamber filled with methane gas, and the γ dose is measured with a graphite chamber filled with CO_2 gas. The fast neutron dose is estimated by subtracting the measured γ dose from the measured total dose. Although this results in high uncertainty in the TE chamber fast neutron dose measurement, uncertainties in the ionization chamber measurements are acceptable due to the low fast neutron contamination of the DM A-BNCT neutron energy spectrum. Figure 20 shows the percentage contribution of the individual dose components, D_N , D_B , D_γ , and D_{fast} in the weighted total brain dose for the phantom, along with the MCNP code simulation. The measured values are agreed well with the MCNP simulation results. The maximum dose appears at the depth of 2.75 cm from the beam port plane, this depth includes the air gap and phantom wall thickness.

The LiCAF detector used for the online epithermal neutron flux is calibrated by the gold wire activation method, and it is checked by comparison with the MCNP calculated expectations. The thermal neutron flux as measured by gold wire activation is compared with the MCNP simulation expectation on the phantom and the neutron beam information previously obtained from the BSA design. If the comparison shows a good

agreement between the measured thermal neutron flux and the calculated flux, it confirms the inferred epithermal neutron flux at the beam port. The neutron count rate from the LiCAF detector is calibrated against the confirmed epithermal neutron flux as a function of the proton beam power (or average beam current). To enhance signal intensity, the body of the LiCAF detector is covered by a polyethylene (PE) tube 23 mm in diameter and 75 mm in length. Figure 21 shows the epithermal neutron flux measured by the LiCAF detector as a function of proton beam power. It shows very good linearity of epithermal neutron flux with the proton beam power as expected. The slope of the linear curve represents the epithermal neutron conversion efficiency of the DM A-BNCT neutron source. That is, $\Phi_{\text{epi}}/P_b = 5 \times 10^7 \text{ n/cm}^2\cdot\text{s/kW}$, which was very high compared to other A-BNCT neutron sources. The measured epithermal neutron flux is $1 \times 10^9 \text{ n/cm}^2\cdot\text{s}$ at 20 kW beam power. Online epithermal neutron flux measurement is also shown in Fig. 21.

4 Pre-clinical study

The BNCT therapeutic efficacies in vitro and in vivo experiments have been studied at the DM A-BNCT facility. The results were published very recently [50]. For evaluation of the efficacy of BNCT, U-87 MG cells were selected as representative brain cancer, and FaDu and SAS cell lines were chosen for head and neck cancers for in vitro study. And U-87 MG xenograft model is selected in vivo study.

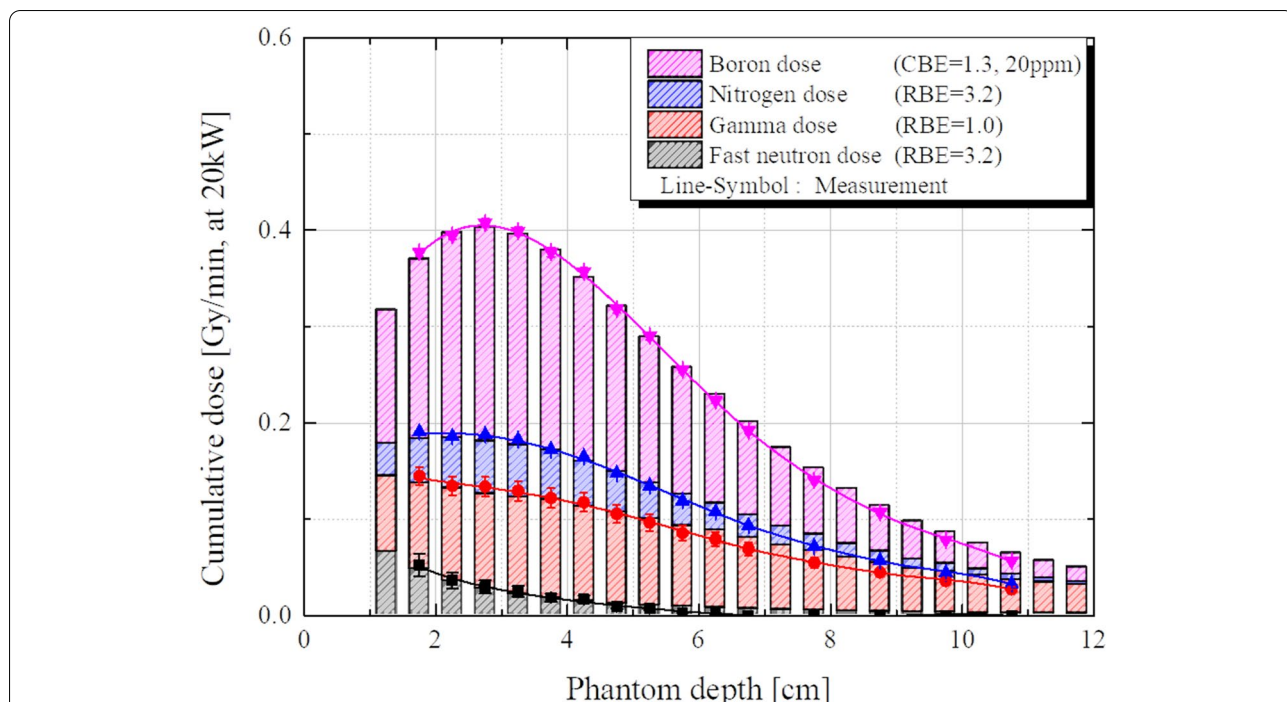


Fig. 20 Percentage contribution of individual dose components (D_N , D_B , D_γ , and D_{fast}) to the weighted total brain dose, as a function of depth along the central axis inside the phantom. Proton linac operating at 20 kW. The first 10 mm in the phantom is the thickness of water behind the beam port plane; an air gap and then the phantom wall thickness. The phantom was irradiated with an epithermal neutron flux of 1×10^9 n/cm²·s which was confirmed by neutron activation. The brain is assumed to have a ¹⁰B concentration of 20 ppm in normal tissues, a nitrogen mass percentage of 2.22 for the thermal neutron dose, and a hydrogen mass percentage of 10.7 for the fast neutron dose. The weighting factors are RBE = 3.2 for D_N and D_{fast} , RBE = 1 for D_γ , and CBE = 1.3 for D_B

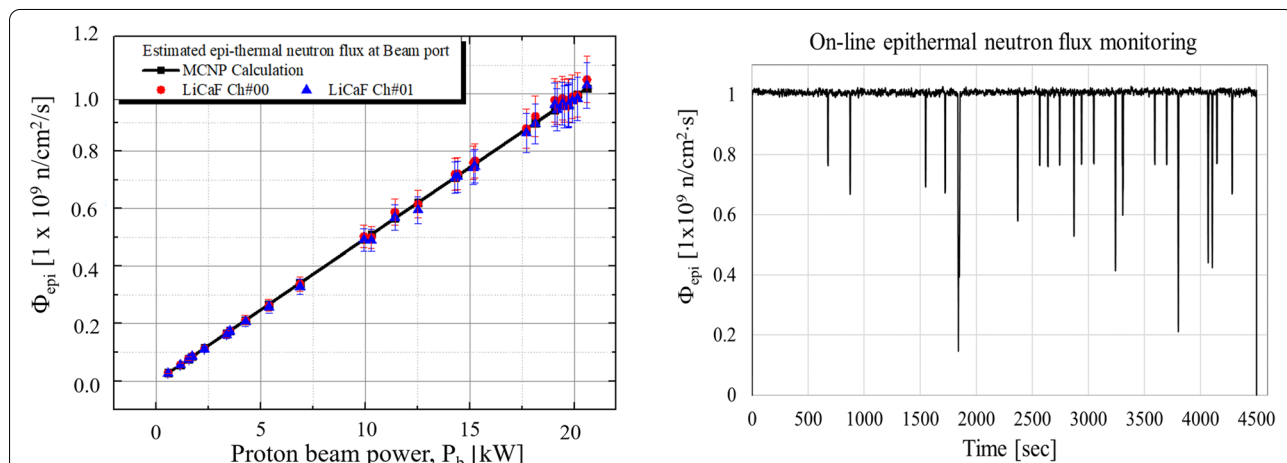


Fig. 21 (Left) Epithermal neutron flux as a function of proton beam power and (right) real-time epithermal neutron flux monitoring during a 75-min irradiation test at 20 kW beam power (10 MeV and 2 mA)

For the in vitro study, ¹⁰B-enriched boronophenylalanine (BPA) uptake by the cells was measured, and then, the cells were irradiated by neutrons. The intracellular boron concentration levels from highest to lowest using SAS, FaDu, and U-87 MG were measured, respectively.

After neutron irradiation, cell viability was observed by clonogenic assays to evaluate the BNCT therapeutic efficacy. For cell irradiation, the U-87 MG, FaDu, and SAS cells were treated with two different BPA concentrations of 500 and 1000 μ g/mL for 3 h. Cells were located 5 cm

in front of the acrylic phantom to be irradiated by thermal neutrons. The irradiation session was planned with three different thermal neutron fluences of 2, 3, and 4 × 10¹¹ n/cm². The survival fractions of the U-87 MG cells were 0.358, 0.274, and 0.196 in the 500 µg/mL treatment group and 0.182, 0.132, and 0.084 in the 1000 µg/mL treatment group. The survival fractions of the FaDu cells were 0.087, 0.022, and 0.008 in the 500 µg/mL treatment group and 0.025, 0.008, and 0.002 in the 1000 µg/mL treatment group. The survival fractions of the SAS cells were 0.056, 0.020, and 0.004 in the 500 µg/mL treatment group and 0.012, 0.003, and 0.001 in the 1000 µg/mL treatment group. Thus, for the U-87 MG, FaDu, and SAS BNCT groups, the results showed that the survival fractions were decreased proportionally depending on BPA treatment concentration and neutron irradiation dose. Figure 22 shows the results of in vitro test for the FaDu cell, which is selected from the reference [50].

In in vivo study, the boron concentration in the tumor, blood, and skin on the U-87 MG xenograft model was measured, and tumor growth rate was obtained from measurements of the tumor volumes in the untreated (no BPA and no neutron irradiation) control group (G1) and all the irradiated groups (G2~G5) over 4 weeks from the irradiation day. In the untreated control group (G1) and neutron irradiation group without BPA administration (G2), rapid tumor growth was observed with the average tumor volumes at 4 weeks after neutron irradiation being 1633.2 mm³ and 1150.3 mm³. But in group 3 (G3) which had a neutron irradiation equivalent to a skin dose of 4 Gy-Eq, a significant decrease in tumor volume was observed from the 13th day, and the tumor volume was 307.9 mm³ at 4 weeks after irradiation. Groups 4 and 5 with skin doses of 5 and 6 Gy-Eq each had a significant decrease in tumor volume from the 6th and 8th days,

respectively. Figure 23 shows the in vivo test results from reference [50].

From the in vitro and in vivo studies, a good therapeutic effect of DM A-BNCT was observed. DM A-BNCT will be a treatment option for patients with uncontrolled cancer or no alternative therapy such as glioblastoma.

5 Preparation for clinical trials

Patient safety is the most significant aspect in initiating clinical trials. Therefore, various preparations and validations are essential before BNCT clinical trials. For clinical use, on the technical side, a treatment planning system (TPS), a patient positioning system, and a validated pharmacokinetic (PK) simulation platform have to be ready. And all clinical trials should be regulated under the pharmaceutical act and the medical device act and be reviewed by IRB (Institutional Review Board) for patient's safety. Therefore, medical staff and sponsors intent on initiating clinical trials should submit safety and efficacy data of medical devices and drugs and follow the numerous administrative steps required by regulating authorities. Most of all, adequate communications with regulatory authorities are recommended prior to BNCT clinical trials.

5.1 Treatment planning

The patient treatment is planned using a treatment planning system (TPS) and PK simulation to determine the ¹⁰B dose and the irradiation time. An in-house treatment planning system (TPS) has been developed for DM A-BNCT. The main role of TPS is to calculate the doses in the human body and to find the optimal neutron beam direction for aiming to the tumor site. The dose calculation is based on the existing Monte Carlo seraMC engine code [51]. The original seraMC engine has been modified

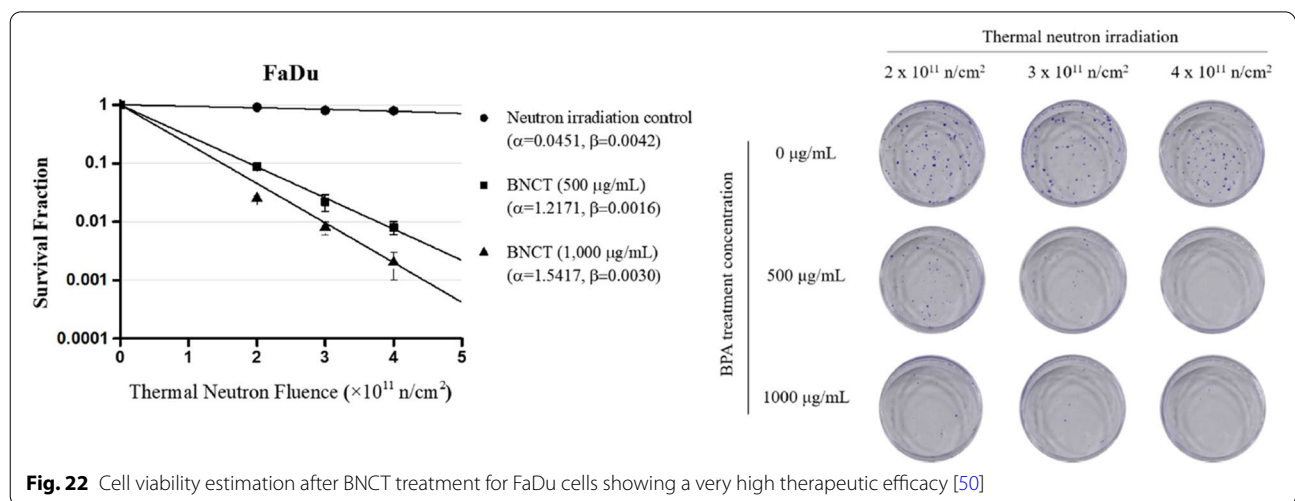


Fig. 22 Cell viability estimation after BNCT treatment for FaDu cells showing a very high therapeutic efficacy [50]

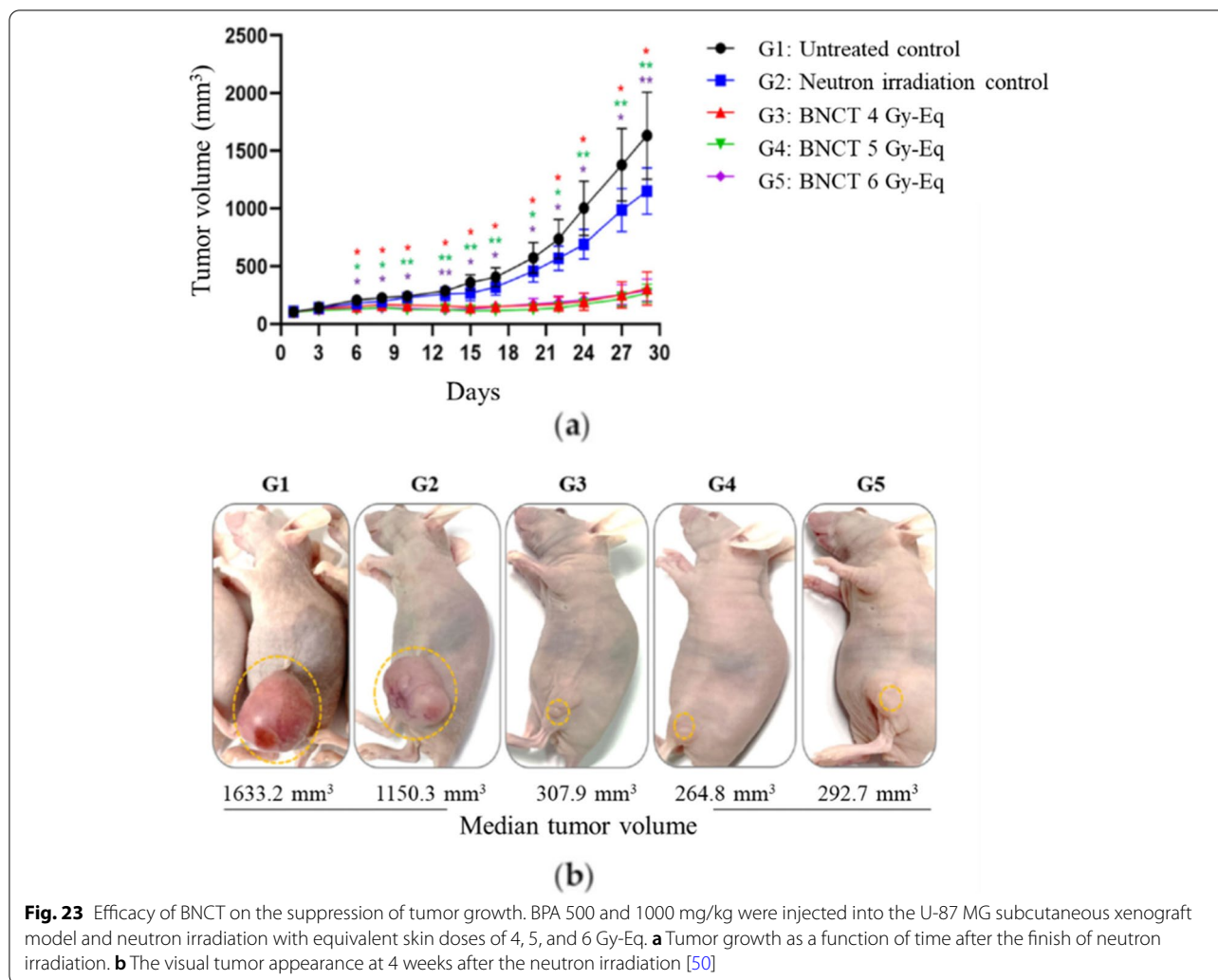


Fig. 23 Efficacy of BNCT on the suppression of tumor growth. BPA 500 and 1000 mg/kg were injected into the U-87 MG subcutaneous xenograft model and neutron irradiation with equivalent skin doses of 4, 5, and 6 Gy-Eq. **a** Tumor growth as a function of time after the finish of neutron irradiation. **b** The visual tumor appearance at 4 weeks after the neutron irradiation [50]

and upgraded to run on a modern parallel computing server. The TPS then calculates the total dose which is converted to “monitor units (MU),” and termination limits are set to end the neutron irradiation after the prescribed dose has been delivered. In DM A-BNCT clinical planning, 1 MU is defined as the neutron fluence of 3×10^{10} n/cm². In this definition, delivering a dose of 1 MU requires an irradiation time of 30 s assuming the epithermal neutron flux is 1×10^9 n/cm²·s at the BSA beam port. But it is important to accurately predict ¹⁰B concentration in the blood during neutron irradiation to confirm or correct the number of MUs and when the neutron irradiation starts. The number of MUs and the neutron irradiation starting time after the end of BPA injection are corrected by measuring the blood ¹⁰B concentration using ICP-MS spectroscopy during and after BPA injection and subsequent estimation of blood ¹⁰B concentration during irradiation by PK simulation. The TPS includes also many advanced user interface functions to

facilitate precise and safe planning of the operation. It offers interactive and quantitative image displays, and beams-eye-view displays, along with the usual data input and output and graphics interface features common to existing radiotherapy TPS.

5.2 Patient positioning

Since the neutron beam line and the treatment room are on the same horizontal plane, patients can be treated in either a sitting or lying position. Two X-ray systems are used to confirm the patient has been positioned as determined by the treatment plan. A multi-axis rotatable positioning bed and a distance-measuring multi-laser instrument are used to perform this accurately. The X-ray images are compared with radiography images of desired tumor position digitally reconstructed by the TPS program. Once the patient is situated in the treatment position, several points, “regions of interest (ROIs)” on the patient are monitored in real time during treatment using

a multiple camera system with motion capture software. This is referred to as the motion monitoring system (MMS). The three-dimensional coordinates of each point on a patient can be followed in real-time during the neutron irradiation, which is a reference factor to control the TPS system not to exceed the planned therapeutic radiation dose depending on the patient's movement.

6 Summary

The boron neutron capture therapy (BNCT) is considered as an attractive new concept of cancer treatment. The BNCT clinical trials have been performed using neutron beams from the research reactor in the past. Nowadays, the BNCT facility is under development and commissioned using accelerator-based neutron sources, so-called A-BNCT. The first A-BNCT is a cyclotron-based BNCT that has been operating for patient's treatment in a hospital in Japan since 2020. Taking consideration of the physics and engineering issues in neutron production based on the accelerator, various types of the accelerator are under development around the world. In Korea, DawonMedax has developed an A-BNCT facility for clinical use using a proton linear accelerator (LINAC) and beryllium target. The LINAC is designed with a proton beam energy of 10 MeV and an average current of a maximum of 4 mA. The LINAC design consists of a duo-plasmatron ion source, low-energy beam transport (LEBT), radio-frequency quadrupole (RFQ) linac, drift tube linac (DTL), and beam transport line (BTL) which are followed by a thin beryllium target and beam shaping assembly (BSA) for epithermal neutron beam generation. The epithermal neutron flux from the BSA is more than the IAEA-recommended value (1×10^9 n/cm²·s) at just a 2-mA averaged beam current. All the neutron beam parameters satisfy their IAEA recommendations except the fast neutron component whose dose ratio is slightly higher than the recommended value. Significant BNCT efficacy was observed in pre-clinical studies. Our neutron beam quality was good enough to reveal the good therapeutic effect of BNCT. The results of pre-clinical studies validated the comprehensive binary therapy of both boron drug and DM A-BNCT. Based on these safety and efficacy data, BNCT clinical trials have been permitted in the BNCT center located at Songdo in Incheon. The first clinical trial is a multi-centered radiation dose escalation, open, exploratory, phase 1/2a clinical trial on the safety and efficacy, and pharmacokinetic characteristics of BNCT in patients with recurrent high-grade glioma. The primary endpoint of phase 1 is the safety and tolerability of BNCT to determine dose-limiting toxicity and define the maximum tolerated dose. The primary

endpoint of the phase 2a trial is to evaluate 6-month progression-free survival by modified Response Assessment in Neuro-Oncology (RANO) criteria. In addition to high-grade glioma, various solid cancers will be indications for BNCT clinical trials including locally recurrent head and neck cancers, hepatic cancer, lung cancer, breast cancer, and melanoma. Most of all, multiple beam lines of BNCT facility are preferable to operate efficiently in a hospital. More than two treatment rooms will reduce the waiting time for the patient's preparation and increase the number of treated patients in a day. For this reason, a second beamline will be installed at the BNCT center. And the facility can be also devoted to testing the new-generation boron carrier compounds, which are under development by DawonMedax. As well as the clinical use of BNCT, a neutron-generating system can be used as a testing device to evaluate integrated circuits and discrete semiconductor memory devices using thermal neutron irradiation [52].

In the future, low-energy and low-power accelerators are preferred for A-BNCT concerning the radiation exposure to the full-time staff and patients during a long period of treatment in the hospitals. Also, when parts of the accelerator machine including the target are disassembled for maintenance and future upgrades, and when the facility reaches the end of life, the entire facility is decommissioned. Therefore, it is worth stressing the importance of minimization of activation levels. From these points of view, we need to study how the accelerator beam energy can be reduced keeping sufficient epithermal neutron flux with the beryllium target. The easy way is to increase the average beam current to reduce the accelerator energy although the high-current operation in the LINAC is challenging. In addition, judicious materials selection of BSA will be needed to mitigate neutron activation because neutrons will activate isotopes in almost any element. This is also a very challenging task because the material selection is quite limited by the requirement of IAEA-recommended neutron parameters. Therefore, good training of radiation workers and staff is very important for the management of radiation exposure. On the other hand, when the next-generation boron agency is developed with higher ¹⁰B delivery efficiency to the cancer cells, the accelerator energy can be significantly reduced under the same treatment time condition using the lower epithermal neutron flux. The other way is to reduce the treatment time with high epithermal neutron flux and 8 to 10 MeV accelerator beam energy. To reduce both the treatment time and accelerator energy, very high ¹⁰B delivery efficiency is anticipated for the future prospects of ideal radiotherapy of BNCT.

Acknowledgements

At the beginning of the A-BNCT project, the design of the RF linac, neutron moderator, and facility shielding structure was done in collaboration with Prof. Eun-San Kim Group at Korea University Sejong Campus, Dr. Jeong Yeon Hwang Group at Pohang Accelerator Laboratory, Dr. Byung Sub Lee Group at the Korea Basic Science Institute, and the Cheol Woo Lee Group at the Korean Atomic Energy Research Institute. We would like also to thank Emeritus Professors Won Namkung and Moohyun Cho from POSTECH, and Hiroshi Matsumoto from KEK for their valuable comments and discussions.

Authors' contributions

The authors "Dong-Su Kim, Je-Un Han, Hyung Jin Yoon, Jung Jin Hwang, Ju Jin Kim, Yoo Soon Jang, Seok Chang Han, Woong Hee Kim, Do Goo Kang, Hyun Jin Seo, Soo Young Lee, Na Hyung Park, Myeng Hyun Lee, Sung June Bae, Seung Hoon Lee, Gyu Ho Cho, Seong Han Kim, Seong Hwan Moon, and Min Kyu Lee" worked for the development of the accelerator-based neutron source and evaluation of the accelerator performance. The author "Byung Hyo Woo" contributed to the design of the beam-shaping assembly to meet the IAEA recommendation of neutron beam parameters suitable for BNCT. Neutron dosimetry data and its relevant analysis were carried out by the neutron dosimetry group "Sang June Jeon, Jae Won Choi, and Kyu Young Lee." Dong Seok Huh and Dong Woo Kim worked for the license of a neutron source facility to use for the medical application. Other authors worked on the medical research activities such as pre-clinical study and preparation of clinical trials in later sections of this manuscript. The author(s) read and approved the final manuscript.

Funding

The accelerator-based BNCT (A-BNCT) project, "Development of a system capable of performing a proton linear accelerator-based BNCT within an hour" (task number 10063465), was funded by the Ministry of Trade, Industry, and Energy from June 2016 to the end of 2021.

Availability of data and materials

Most of the supporting data cannot be shared because this topic is related to a matter of confidential business.

Declarations

Ethics approval and consent to participate

Not applicable.

Consent for publication

Not applicable.

Competing interests

The authors declare no competing interests.

Author details

¹Accelerator Department, Dawonsys, Ansan 15655, Korea. ²DawonMedax, Seoul 06735, Korea.

Received: 22 September 2022 Accepted: 14 October 2022

Published online: 27 October 2022

References

- W. A. G. Sauerwein et al. (eds.), *Neutron Capture Therapy-Principles and Applications* ((Springer-Verlag, Heidelberg, 2012)
- E.J. Hall, A.J. Giaccia, *Radiobiology for the Radiologist*, 7th edn. (Lippincott Williams & Wilkins, 2012)
- W.H. Sweet, Early history of development of boron neutron capture therapy of tumors. *J. Neuro-Oncol.* **33**, 19 (1997)
- M.A. Dymova et al., Boron neutron capture therapy: current status and future perspectives. *Cancer Commun.* **40**, 406 (2020)
- R.F. Barth et al., Boron delivery agents for neutron capture therapy of cancer. *Cancer Commun.* **38**, 35 (2018)
- Y. Sakurai, T. Kobayashi, Spectrum evaluation at the filter-modified neutron irradiation field for neutron capture therapy in Kyoto University Research Reactor. *Nucl. Instr. Meth. Phys. Res.* **A531**, 585 (2004)
- L. Provenzano et al., A prospective study to assess the performance of the improved Boron Neutron Capture Therapy Facility in Argentina. *Appl. Radiat. Isot.* **88**, 171 (2014)
- Y.H. Liu et al., Performance evaluation of the source description of the THOR BNCT epithermal neutron beam. *Appl. Radiat. Isot.* **69**, 1892 (2011)
- G. Ke et al., The study of physics and thermal characteristics for in-hospital neutron irradiator (IHNI). *Appl. Radiat. Isot.* **67**(7-8 Suppl), S234 (2009)
- IAEA-TECDOC-1223: Current states of neutron capture therapy (IAEA 2001). https://www-pub.iaea.org/MTCD/publications/PDF/te_1223_pm.pdf
- S.Y. Taskaev, Accelerator based epithermal neutron source. *Phys Part Nuclei* **46**, 956 (2015)
- Y. Kiyonagi et al., Accelerator-based neutron source for boron neutron capture therapy. *Ther. Radiol. Oncol.* **2**, 55 (2018)
- W. Park, S.P. Konish, T.H. Smick, and T. Sakase. Neutron target for boron neutron capture therapy, US Patent No. 62/157,652, filed May 6, 2015, and issued 10 Nov 2016.
- F. Naito, Introduction to accelerators for boron neutron capture therapy. *Ther. Radiol. Oncol.* **2**, 54 (2018)
- Y. Yamagata et al., Development of a neutron generating target for compact neutron sources using low energy proton beams. *J. Radioanal Nucl Chem* **305**, 787 (2015)
- J.F. Ziegler, M.D. Ziegler, J.P. Biersack, SRIM – the stopping and range of ions in matter. *Nucl. Instrum. Meth. Phys. Res. B* **268**, 1818 (2010) <http://www.srim.org/>
- I.M. Kapchinskii, V.A. Teplvakov, A linear ion accelerator with spatially uniform hard focusing. *Prib. Tekh. Eksp. No.* **2**, 19 (1970)
- K.R. Crandall, R.H. Stokes, T.P. Wangler, *RF quadrupole beam dynamics design studies, Proceedings of the 1979 Linear Accelerator Conference* (Montauk, New York, USA, 1979) <https://accelconf.web.cern.ch/l79/papers/s4-1.pdf>
- L.W. Alvarez, The design of a proton linear accelerator. *Phys. Rev.* **70**, 799 (1946)
- L.W. Alvarez et al., Berkeley proton linear accelerator. *Rev. Sci. Instrum.* **26**, 111 (1955)
- T.P. Wangler, *RF Linear accelerators*, 2nd edn. ((WILEY-VCH Verlag GmbH & Co. KGaA, Weinheim, 2008) ch4 & 6
- O. Lawrence, M.S. Livingston, The production of high-speed light ions without the use of high voltages. *Phys. Rev.* **40**, 19 (1932)
- S. Nakamura et al., Evaluation of radioactivity in the bodies of mice induced by neutron exposure from an epi-thermal neutron source of an accelerator-based boron neutron capture therapy system. *Proc. Jpn. Acad., Ser. B* **93**, 821 (2017)
- H. Tanaka et al., Characteristics comparison between a cyclotron-based neutron source and KUR-HWNIF for boron neutron capture therapy. *Nucl. Instr. Meth., Phys. Res. B* **267**, 1970 (2009)
- H. Kumada et al., Development of LINAC-based neutron source for boron neutron capture therapy in University of Tsukuba. *Plasma Fusion Res.* **13**, 2406006 (2018)
- L. Silvestrin et al., SPES and the neutron facilities at Laboratori Nazionali di Legnaro. *Eur. Phys. J. Plus* **131**, 72 (2016)
- C. Ceballos et al., Towards the final BSA modeling for the accelerator-driven BNCT facility at INFN LNL. *Appl. Radiat. and Isotopes* **69**(12), 1660 (2011)
- Y. Kiyonagi et al., Status of accelerator-based BNCT projects worldwide. *AIP Conf. Proc.* **2160**, 050012 (2019). <https://doi.org/10.1063/1.5127704>
- K. Watanabe, First experimental verification of the neutron field of Nagoya University Accelerator-driven neutron source for boron neutron capture therapy. *Appl. Radiat. And Isotopes* **168**, 109553 (2021)
- V. Kanygin et al., In vivo accelerator-based boron neutron capture therapy for spontaneous tumors in large animals: case series. *Biology* **11**, 138 (2022)
- L. Porra et al., Accelerator-based boron neutron capture therapy facility at the Helsinki University Hospital. *Acta Oncologica* **61**, 269 (2021)
- I. Porras et al., Applied radiation and isotopes. *Appl. Radiat. and Isotopes* **165**, 109247 (2020)

33. P. Torres-Sánchez et al., Optimized beam shaping assembly for a 2.1-MeV proton-accelerator-based neutron source for boron neutron capture therapy. *Sci. Rep.* **11**, 7576 (2021)
34. P. Michael et al., A 50 kW liquid-lithium target for BNCT and material-science applications. *EPJ Web of Conf.* **231**, 03004 (2020)
35. D.S. Kim et al., Development of the accelerator based boron neutron capture therapy system for cancer treatment within 1 hour therapeutic time, 17th International Congress on Neutron Capture Therapy (2016).
36. C.-H. Lee et al., Status of development and planning activities on CANS in Korea. *J. Neutron Res.* **23**, 2-3, 127 (2021)
37. J. Bahng et al., *Development of RFQ for BNCT accelerator, Proceedings of IPAC2017, THPIK073* (Denmark, Copenhagen, 2017) <https://accelconf.web.cern.ch/ipac2017/papers/thpik073.pdf>
38. D. Uriot, N. Pichoff, *Status of TraceWin code* (Proceedings of IPAC2015, MOPWA008, Richmond) <https://accelconf.web.cern.ch/ipac2015/papers/mopwa008.pdf>
39. C.J. Werner et al., MCNP6.2 Release notes-report LA-UR-18-20808 (Los Alamos National Laboratory (LANL)), (2018) <https://mcnp.lanl.gov/>
40. I.H. Seo, S.H. Kim, *Study of BNCT biological effect at out-of-field region, internal report of DawonMedax* (2021)
41. J.W. Wilson et al., Implementation of Gy-Eq for deterministic effects limitation in shield design. *J. Radiat. Res.* **43**(Suppl), S103–S106 (2002)
42. W. Jaschke et al., Radiation-induced skin injuries to patients: what the interventional radiologist needs to know. *Cardiovasc Intervent Radiol.* **40**(8), 1131 (2017)
43. M. Herve, N. Sauzet, D. Santos, On the epithermal neutron energy limit for accelerator-based boron neutron capture therapy (AB-BNCT): study and impact of new energy limits. *Physica Medica* **88**, 148 (2021)
44. P. Binns, K. Riley, O. Harling, *Research and development in neutron capture therapy, Proceedings of 10th International Congress on Neutron Capture Therapy* (Essen, 2002)
45. O. Kononov et al., Optimization of an accelerator-based epithermal neutron source for neutron capture therapy. *Appl. Radiat. Isot.* **61**, 1009 (2004). <https://doi.org/10.1016/j.apradiso.2004.05.028> (Topics in Neutron Capture Therapy: Proceedings of the Eleventh World Congress on Neutron Capture Therapy (ISNCT-11))
46. Y.-W. Liu et al., Renovation of epithermal neutron beam for BNCT at THOR. *Appl. Radiat. Isot.* **61**, 1039 (2004). <https://doi.org/10.1016/j.apradiso.2004.05.042> (Topics in Neutron Capture Therapy: Proceedings of the Eleventh World Congress on Neutron Capture Therapy (ISNCT-11))
47. V. Giusti et al., Monte Carlo model of the Studsvik BNCT clinical beam: description and validation. *Med. Phys.* **30**, 3107–3117 (2003). <https://doi.org/10.1118/1.1626120>
48. B. J. Mijneer et al., ICRU Rept 45: Clinical Neutron Dosimetry Part I: Determination of Absorbed Dose in a Patient Treated by External Beams of Fast Neutrons. *J. ICRU.* **23**(2) (1989)
49. M. Reginatto, P. Goldhagen, S. Neumann, Spectrum unfolding, sensitivity analysis and propagation of uncertainties with the maximum entropy deconvolution code MAXED. *Nucl. Instr. and Meth. A* **476**, 242 (2002)
50. I.H. Seo et al., The anti-tumor effect of boron neutron capture therapy in glioblastoma subcutaneous xenograft model using the proton linear accelerator-based BNCT system in Korea. *Life* **12**, 1264 (2022)
51. D. Nigg et al., SERA – an advanced treatment planning system for neutron therapy and BNCT. *Trans Am Nucl Soc.* **80**, 223 (1999)
52. Y. Kiyonagi, Neutron applications developing at compact accelerator-driven neutron sources. *AAPPS Bull.* **31**(1), 22 (2021)

Publisher's Note

Springer Nature remains neutral with regard to jurisdictional claims in published maps and institutional affiliations.